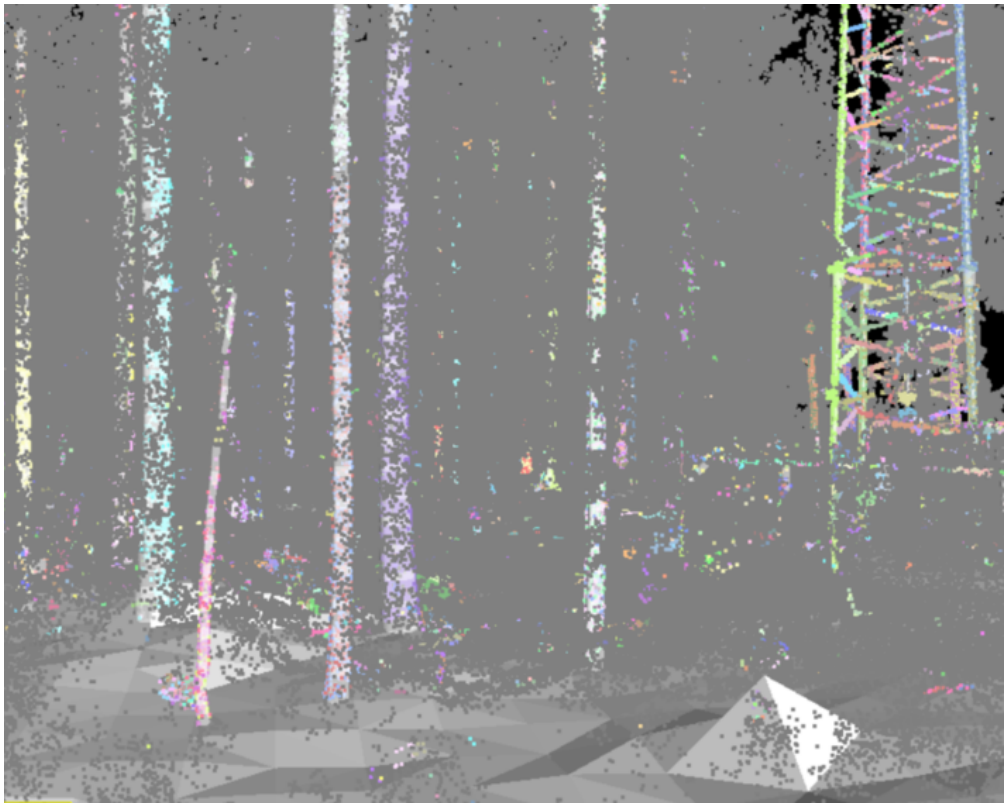

Electromagnetic Scattering Model of a Laser-scanned Forest

Master's thesis in Wireless, Photonics and Space Engineering

Dennis Gustavsson

Department of Space, Earth and Environment
Division of Microwave and Optical Remote Sensing

CHALMERS UNIVERSITY OF TECHNOLOGY
Gothenburg, Sweden 2019

Master's thesis 2019

Electromagnetic Scattering Model of a Laser-scanned Forest

Dennis Gustavsson

CHALMERS
UNIVERSITY OF TECHNOLOGY

Department of Space, Earth and Environment
Chalmers University of Technology
Gothenburg, Sweden 2019

Electromagnetic Scattering Model of a Laser-scanned Forest
Dennis Gustavsson

Supervisors: Albert Monteith, Lars Ulander Department of Space, Earth and Environment and Hans Hellsten, Saab Surveillance
Examiner: Lars Ulander, Department of Space, Earth and Environment SE-412 96 Gothenburg

Master's Thesis 2019
Department of Space, Earth and Environment
Division of Microwave and Optical Remote Sensing
Chalmers University of Technology

Cover: Lidar measurements of a forest.

Typeset in LaTeX

Gothenburg, Sweden 2019

Electromagnetic Scattering Model of a Laser-scanned Forest

Dennis Gustavsson
Department of Space, Earth and Environment
Chalmers University of Technology

Abstract

There exists a lot of research on how to use radar to measure forest properties, like the forest's biomass. Knowledge about a forest's biomass can then be used to determine whenever or not it is time to cut down the trees in the forest. There are also environmental reasons for knowing the biomass of a forest on a global scale, where the total biomass in the forest relates to the carbon cycle. However, there are multiple forest parameters besides the biomass that affects the forest backscattering and this may give inconsistencies when estimating the biomass at different locations. The goal of this thesis was to study how different forest parameters affect the radar backscattering by creating an electromagnetic model of a forest area, and perform computations of the backscattering of incident radar waves for frequencies in the VHF and UHF bands. To accomplish this, LIDAR data from SLU (The Swedish University of Agricultural Sciences) was used. The trees in the forest were modelled as a sum of cylinders placed on top of one another to approximate the trees and the forest.

The scattering for a single cylinder can be calculated either with the truncated infinite cylinder approximation or Generalized Rayleigh-Gans approximation. By also considering possible ground reflections in combination with the scattering at the cylinders, the total backscattering of the incident wave can be computed for a single cylinder placed above the ground. The total scattering from a tree or a forest, which is built up of multiple cylinders, can then be calculated as a sum of the backscattering amplitude from each cylinder.

As expected, the computed radar cross section (RCS) is shown to be different depending on the polarization of interest for the incident and reflected radar waves. A clear connection between the size of the trees and the RCS was found. The RCS for a single tree in the forest is also shown to be sensitive to small changes in the ground slope or the tree's inclination. It could also be seen that when the number of cylinders used to approximate a tree increases, the more the RCS fluctuates with the frequency. However, the fluctuations are around the same RCS values as the calculated RCS for tree models with fewer cylinders.

For the forest it is observed that small changes in antenna position and small changes to the approximation of the tree geometry barely changes the averaged backscattering. The computations on the forest model gives consistent results but there is currently not possible to judge how well the computed backscattering matches reality. Some differences compared to the real forest backscattering is expected due to simplifications and approximations. An example is that the backscattering from the needles and branches have been neglected.

Acknowledgements

First of all, I am very grateful to Lars Ulander and Hans Hellsten who have been my supervisors for this thesis work. They have helped and encouraged me a lot during my work. This project was also supervised by Albert Monteith that has helped me to get some computer program to work and provided me with support when using this program. I would also like to extend a warm thanks to SLU, The Swedish University of Agricultural Sciences, who helped me by providing LIDAR and cylinder data which I have used in my thesis work.

Furthermore, I would like to express my gratitude to Chalmers University of Technology and all the teachers I met during my time as a student at this fantastic university. Without the knowledge they have conveyed to me, this work could not have been carried out by me.

Last, but not least, I want to express my gratitude for all the support and all the encouragement I have received from my parents and grandparents during the time I have been studying. They have helped and supported me in my studies right from pre-school to university - thanks.

Dennis Gustavsson, Gothenburg, 05-2019

Contents

1
Introduction

In recent years, the interest in using remote sensing to determine various properties of forests has increased. Since all forms of observations that observes an object's properties without touching it can be called remote sensing, this is a very broad subject. This means that man's sight, which the woodcutter has used for many years, can be the oldest remote sensing method used to determine different properties of a forest. However, using the human sight to determine a forest's properties takes time and can be difficult to succeed with for an inexperienced individual. To find methods to determine various properties of a forest in an efficient and simple way, research towards using radar to study large forest areas have become increasingly popular.

For a remote sensing system to be useful, it is not only necessary that it can determine the target's properties, but also that the information about these properties are useful. The information received from a remote sensing system when studying a forest can be used to decide how to maintain the forest or estimate a reasonable selling price. For example, an important property for a forest is it's biomass, and the information about the biomass can be used to determine, whenever or not, it is time to cut down the trees in the forest. In the case one wants to buy or sell a forest area, the biomass of the trees in the area may also be a factor in determining the forest value. But there are also environmental uses in knowing the biomass of a forest on a global scale, where the total biomass in the forest relates to the carbon cycle.

There exists a lot of research on how to use radar to measure forest properties or on how to create forest images using radar. For example [1] writes about how to estimate biomass using radar and the research in [2] concerns radar imaging.

Radar systems work by transmitting electromagnetic waves in the form of pulses containing multiple frequencies. Today, the used wavelength can vary from tens of meters to a few millimeters. In the early days of the radar system, it worked by transmitting electromagnetic pulses and measuring the time it took for the pulse to come back, and based on that determining a distance to an object. However, since then multiple new applications for the radar have been found, such as identifying and tracking objects or creating images of an area showing how some of the area's properties varies [3].

The radar's measurements have also proved useful in other more specialized areas. An example is to study the relation between a forest's backscattering of radar signals and the biomass of the forest above the ground level. There are however multiple forest parameters besides the biomass that affects the backscattering and this may give inconsistencies when estimating the biomass at different locations.

Such parameters are what kind of trees the forest contains, the slope of the ground and the inclinations of the trees, rocks and other non-tree objects which can be found in the forest. These parameters may affect the backscattering without giving information about the biomass. Therefore, it is important to understand how not just the biomass relates to the backscattering, but also to know how the other forest parameters relates to it.

The goal of this thesis was to study how the backscattering changes when the ground/tree inclination changes or when other parameters change. We will also study how the backscattering depends on the tree and forest model used. This will be done by creating an electromagnetic forest model in Matlab and compute the backscattering for trees and a forest area under various conditions.

To find out how the backscattering changes when the ground/tree inclination changes, an electromagnetic forest model and five single tree models have been created in Matlab. Using the forest model and the single tree models the backscattering for incident electromagnetic waves were computed. The computation was made using one of two different approximations methods. One is the truncated infinite cylinder and the other the Generalized Rayleigh-Gans (GRG) approximation. The computations were made for different situations that may occur in a forest and the parameters, like the tree inclination and ground slope, were varied for frequencies in the VHF and UHF bands.

Before creating an electromagnetic forest model, a geometrical forest model needs to be created. The geometrical forest model was created from LIDAR (Light detection and ranging) data collected by SLU (The Swedish University of Agricultural Sciences) using terrestrial laser scanning (TLS). SLU also processed the data to cylinders representing the stems using the methods described in [4]. The trees in the forest were then modeled as cylinders using those measurement data and a tree model [5], that describes the shape of trees. The electromagnetic properties were then added to the trees in the geometrical forest model. This is done with the help of already performed research about electromagnetic properties of trees in [6] and the electromagnetic properties of the ground which is described in [7].

To compute how the created electromagnetic forest model scatters incoming radio waves, and how the scattering changes when different forest parameters are changed, scattering theory from multiple sources were used. The theory of how the electromagnetic wave scatters by one of the cylinders that forms the trees in the forest was calculated using the scattering theory and models from [8], [9] and [10]. Other literature concerning scattering theory is [11] and [12] that present some limitations of the scattering models used in this thesis. The total backscattering was then approximated for the forest model by taking the sum of the scattering from all cylinders. Theory and ideas were also taken from [13] and [14] to produce a method that compensates for the inclination of the cylinders and ground. The cylinders have an inclination if the trees are not standing vertical.

1.1 Societal, ethical and ecological aspects

The computational model used is based on derivations from the closed-form electromagnetic scattering descriptions of simple shapes. The model therefore is not

a full-wave solver, i.e. it does not numerically solve Maxwell's equations such as the method of moments or finite element method. These methods would require an immense amount of computing power for the same problem. For the selected frequency range and forest type, the model yields solutions to scattering problems after far fewer computations than a full-wave solver would require. This reduces the energy consumption necessary for computing backscattering from the forest. Sense this project is computer based, it will not give any environmental damage (except for the small amount of energy used to run the computer). The project may in the future be helpful in forest managing but no social or ethical consequences have been identified.

The source of models and equations is cited and it is clearly stated when models/equations have been provided without a source or proof. No other ethical consequences of this work have been identified.

2
Theory

The simulation of an electromagnetic model of a forest requires extensive knowledge of electromagnetic field theory, radar concepts and radar scattering which therefore will be introduced in this chapter. The electromagnetic field theory will be used to explain how radio waves reflect off surfaces. Radar concepts and radar scattering models can approximate the scattering that occurs when a radio wave travels through a forest and be useful when evaluating the forest model.

2.1 Electromagnetic field theory

The electromagnetic field theory describes how a electric (**E**) and magnetic (**H**) fields are created and changed due to the surrounding environment. The changes in the **E** and **H** fields can be described with Maxwell's equations compiled in 1865 [15]. Originally, Maxwell's equations contained 20 unknown variables that where solved with 20 equations. Nowadays it is more usual to use four equations which are considered the main part of Maxwell's equations. Under the assumption of a homogeneous, isotropic and linear medium, Maxwells four equations can be written as [16], [17]

$$\nabla \cdot \mathbf{E} = \rho/\epsilon \tag{2.1a}$$

$$\nabla \cdot \mathbf{H} = 0 \tag{2.1b}$$

$$\nabla \times \mathbf{E} = -\mu \frac{\partial \mathbf{H}}{\partial t} \tag{2.1c}$$

$$\nabla \times \mathbf{H} = \mathbf{J} + \epsilon \frac{\partial \mathbf{E}}{\partial t}. \tag{2.1d}$$

In these equations **J** represent the free current density and ρ represent the free electric charge density. The constant ϵ represents the permittivity and μ represent the permeability for the actual medium.

Usually an electrical field that propagates through a medium can be referred to as an electromagnetic wave. By then using equation (2.1) under the assumption that the electromagnetic wave is sinusoidal, the medium is source free and nonconducting meaning that the variables **J** and ρ are zero, Helmholt's equation that describes how an electromagnetic wave travels through the medium can be derived [17]. This equation is given by

$$\nabla^2 \mathbf{F} e^{jwt} + \mathbf{k}^2 \mathbf{F} e^{jwt} = 0, \tag{2.2}$$

where $\mathbf{F}$ can represent either $\mathbf{H}$ or $\mathbf{E}$ and $\mathbf{k} = (k_x\hat{\mathbf{x}} + k_y\hat{\mathbf{y}} + k_z\hat{\mathbf{z}})$ is the wave vector which gives the direction in which the electromagnetic wave is traveling. The magnitude of the wave number is $k = \sqrt{k_x^2 + k_y^2 + k_z^2} = \omega\sqrt{\epsilon\mu}$ where ω is the sinusoidal angular frequency of the electromagnetic wave.

The solution to Helmholt's equation (2.2) can be written as [18].

$$\mathbf{E}(x, y, z) = \mathbf{E}_0 e^{j\omega t - j\mathbf{k}\cdot\mathbf{R}} \tag{2.3}$$

where $\mathbf{R}$ represents the propagation of the wave traveled in the traveling direction $\hat{\mathbf{k}} = \mathbf{k}/k$ and E_0 is the electrical field when $t = 0$ and $\mathbf{R} = 0$. This expression gives the electrical field at all points in time and space assuming a free space environment. When a electromagnetic wave propagates in a homogeneous medium it travel in a straight path but if a wave encounters objects of other materials the wave will be scattered. Therefore equation (2.3) will need to be complemented with equations describing the scattering of the electromagnetic wave at material borders for a more complete description of wave propagation.

2.2 Reflection off a surface

When an electromagnetic wave propagates into a dielectric flat surface part of the wave will be reflected and the other part will be transmitted through the surface. The reflected wave will according to Snell's law of reflection be reflected so that the reflections angle θ_r is equal to the incidence angle θ_i (see Figure 2.1). Assuming the incident wave travels in the direction $\hat{\mathbf{k}}_i$ and the plane's normal is $\hat{\mathbf{n}}_g$ the direction of the reflected wave $\hat{\mathbf{k}}_r$ can be calculated by

$$\hat{\mathbf{k}}_r = \hat{\mathbf{k}}_i - 2\hat{\mathbf{n}}_g(\hat{\mathbf{n}}_g \cdot \hat{\mathbf{k}}_i) \tag{2.4}$$

To determine the transmitted wave's angle, θ_t, one can use Snell's law of refraction [18]

$$\frac{\sin(\theta_t)}{\sin(\theta_i)} = \sqrt{\frac{\epsilon_1}{\epsilon_2}}. \tag{2.5}$$

The transmitted electromagnetic wave's electrical and magnetic fields both have directions that are orthogonal to each other as well as the wave's traveling direction. A wave that has an electrical field $\mathbf{E}$ that is parallel to the ground plane is said to be horizontally polarized and the horizontal component is denoted by E_h. If instead the electrical field $\mathbf{E}$ is orthogonal towards the horizontal polarization, the electrical field is vertically polarized and the vertical component is denoted by E_v. In this thesis the letter h is used to represent the horizontal polarization and the letter v the vertical polarization. Note that, in the general case, the horizontal and vertical components of $\mathbf{E}$ can have different phases so the components E_h and E_v are complex numbers.

One boundary condition is that the horizontal components of the electrical and magnetic field are unchanged at the boundary between materials. Assume, as in Figure 2.1, that the the incoming electrical field ($\mathbf{E}^i$) is horizontally polarized. In this case the polarization of the reflected ($\mathbf{E}^r$) and transmitted ($\mathbf{E}^t$) electrical field

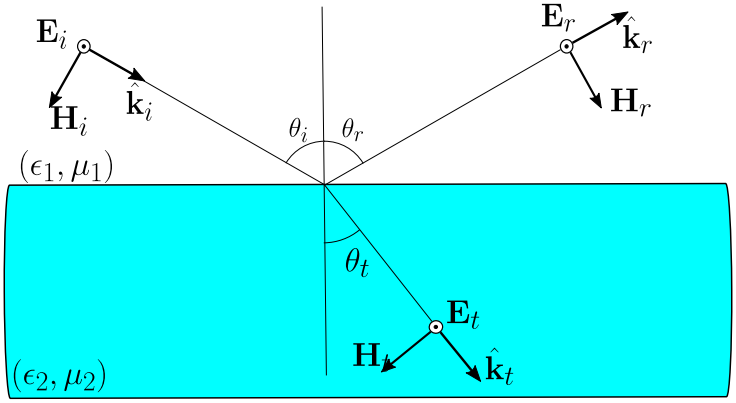

Figure 2.1: A plane wave, with a horizontal electric field polarization, traveling in the $\hat{\mathbf{k}}_i$-direction is reflected and transmitted in a plane boundary between two materials. The different materials in the figure have different permittivity and permeability represented by (ϵ_1, μ_1) and (ϵ_2, μ_2).

will also be horizontally polarized. Using the directions shown in Figure 2.1 the boundary condition can be written as

$$E^i e^{-jk_1 \sin(\theta_i)} + E^r e^{-jk_1 \sin(\theta_r)} = E^t e^{-jk_2 \sin(\theta_t)} \tag{2.6a}$$

$$-\cos(\theta_i) H^i e^{-jk_1 \sin(\theta_i)} + \cos(\theta_r) H^r e^{-jk_1 \sin(\theta_r)} = -\cos(\theta_t) H^t e^{-jk_2 \sin(\theta_t)} \tag{2.6b}$$

where k_1 and k_2 are the wave numbers for the different materials. It is possible to solve equation (2.6) with the help of equation (2.1d) and (2.5). An expression for how much of the wave that is reflected can be derived and this equation is well known as Fresnel's equation, written as [18]

$$\Gamma_{hh} = \frac{\eta_2 \cos(\theta_i) - \eta_1 \cos(\theta_t)}{\eta_2 \cos(\theta_i) + \eta_1 \cos(\theta_t)} \tag{2.7}$$

where $\eta_i = \sqrt{\mu_i/\epsilon_i}$, $i = 1, 2$, is the characteristic impedance of the two materials. The letter combinations hh, vh, hv and vv in the index have a special meaning where the second letter represents the polarization of an incident wave and the first letter the polarization of the reflected wave. In the case of equation 2.7 this means that Γ_{hh} relates the incident and reflected horizontal field component allowing for the reflected horizontal field component to be calculated according to $E_h^r = E_h^i \Gamma_{hh}$.

How much of the wave that is reflected for an incoming wave with a magnetic field polarization perpendicular to the normal can be derived in a similar manner and is calculated as [18]

$$\Gamma_{vv} = \frac{\eta_1 \cos(\theta_i) - \eta_2 \cos(\theta_t)}{\eta_1 \cos(\theta_i) + \eta_2 \cos(\theta_t)}. \tag{2.8}$$

2.3 The radar concepts

Historically, when the radar system was invented they where only capable of detecting targets and determining range but since then the radar system have evolved

[3]. Nowadays radars are also capable of creating images of an area showing how the areas properties wary, identifying and tracking objects. Modern radars are also designed so that they are capable of operating under interference from the environment and other interfering devices and objects. Radar system works by transmitting an electromagnetic wave, such as the one described in (2.3), in a chosen direction. The transmitted wave will when it encounters an object be scatted in all directions causing some of it to be scatted back towards the radar system this scattering is called backscattering. The radar system can then by measuring the time t between sending and receiving a signal calculate the distance (R) to the target as $R = ct/2$ where c is the speed of light.

Important aspects for all radar systems are it's operating center frequency (f_c) and bandwidth (B) that determines the frequency band in which the radar operates. The frequency band is a common way to identifying radar system. There are different definitions of frequency bands but one of the most common is the IEEE standard (std:521-2002) that can be seen in table 2.1.

Table 2.1: The IEEE standard (std:521-2002) designation for the different radar-frequency bands and their nominal frequency range [19].

Band letter designation	Nominal frequency range
HF	3 MHz-30 MHz
VHF	30 MHz-300 MHz
UHF	300 MHz-1000 MHz
L	1 GHz-2 GHz
S	2 GHz-4 GHz
C	4 GHz-8 GHz
X	8 GHz-12 GHz
K_u	12 GHz-18 GHz
K	18 GHz-27 GHz
K_a	27 GHz-40 GHz
V	40 GHz-75 GHz
W	75 GHz-110 GHz
mm	110 GHz-300 GHz

2.4 Radar cross section and scattering

After a radar transmit a pulse, the pulse will propagate through the medium (normally air) before it scatters by an object. The magnitude of the wave that is backscattered towards the radar receiver is dependent on the radar cross section (RCS). While assuming propagation in free space or propagation in air and while neglecting atmospheric attenuation, the power a radar system receives after transmitting a wave can be calculated with the radar equation [3]

$$P_r = \sigma \frac{P_t \lambda^2 G_t G_r}{R^4 (4\pi)^3} \tag{2.9}$$

where R is the distance from the radar transmitter and radar receiver to the scattering object, λ is the transmitted wavelength, P_t and P_r is the transmitted power and the received power respectively, σ is the radar cross section (RCS) of the object, G_t is the gain of the transmitting antenna and G_r is the gain of the receiving antenna. If the same antenna is used to transmit and receive signals the receiving and transmitting gain will be equal ($G_r = G_t$).

In equation (2.9), it can be seen that the strength of the backscattered wave increases as σ increases. It is therefore common to quantify the backscattering strength of a object using the RCS [20], [21] which can be calculated as

$$\sigma = \lim_{R\to\infty} \frac{|E^s|^2}{|E^i|^2} 4\pi R^2, \tag{2.10}$$

where $|E^s|$ is the amplitude of the scatted electrical field a distance R from the object and $|E^i|$ is the incident electrical field strength at the object. This is for the three dimension case and similar definitions for the RCS can be derived for the two and one dimensional case.

The radar cross section σ is not only dependent on the scattering object but also of the waves frequency and polarization. A solution to how cross section depends on the polarization is to derive the RCS for all the desired transmission polarization, but it would be more effective if a general solution to the problem could be found. The solution is the scattering matrix $\mathbf{S}$, see equation (2.11), that differs from the RCS in that it preserve the information about phase and polarization of the wave after scattering

$$\mathbf{S} = \begin{bmatrix} S_{hh} & S_{hv} \\ S_{vh} & S_{vv} \end{bmatrix}. \tag{2.11}$$

The different elements of the scattering matrix describes how different polarization's will be reflected and this allows $\mathbf{S}$ to be used for all incoming polarizations. The elements in the scattering matrix are complex and can therefore affect the polarization of the scatted electrical field whcih can be calculated by [20], [8]

$$\begin{bmatrix} E_h^s \\ E_v^s \end{bmatrix} = \frac{e^{j\omega t - jk_R R}}{R^2} \begin{bmatrix} S_{hh} & S_{hv} \\ S_{vh} & S_{vv} \end{bmatrix} \begin{bmatrix} E_h^i \\ E_v^i \end{bmatrix} \tag{2.12}$$

This gives a more complete description of the scattering process than what can be achieved by using only the RCS (σ). However, radar cross section can be calculated from S by using equation (2.10) and equation (2.12) giving

$$\sigma_{pq} = \lim_{R\to\infty} \frac{|E_p^s|^2}{|E_q^i|^2} 4\pi R^2 = 4\pi |S_{pq}|^2 \tag{2.13}$$

where q and p, respectively can represent horizontal, h, or vertical, v, polarizations. The fact that the the scattering matrix gives more complete description and that one can calculate σ from the scattering matrix, makes $\mathbf{S}$ convenient to use.

2.5 Scattering off objects

When deriving an object's scattering, the form of the object determines whether or not a exact solution can be found. In most case when an exact solution not can

be found an approximation of the solution has to suffice. When exact solution's are derived they are based on Maxwells equations (2.1) and Helmholt's equation (2.2). Only in the cases when an object can be placed in a coordinate system where the object's boundaries coincide with a constant coordinate value is it possible to find an exact solution [21]. A consequence is that the sphere is the only possible three-dimensional finite shape that have an exact solution that can be derived analytically [8]. In this the radius has a constant value. There are however some non-finite forms, like the infinite cylinder, for which the exact solution can be found. In real environments, like forests, shapes like perfect spheres or infinite cylinders are unlikely and therefore approximate solutions to other more usual forms have to be used. Using approximate solution may also in some cases need less computational power while only losing a little accuracy. Both trees and tree branches can be approximated as a number of cylinders that are place on top off each other forming a similar shape to a tree or tree branch. Two methods to approximate finite cylinder are the generalized Rayleigh-Gans estimation (GRG) and the truncated infinite cylinder approximation.

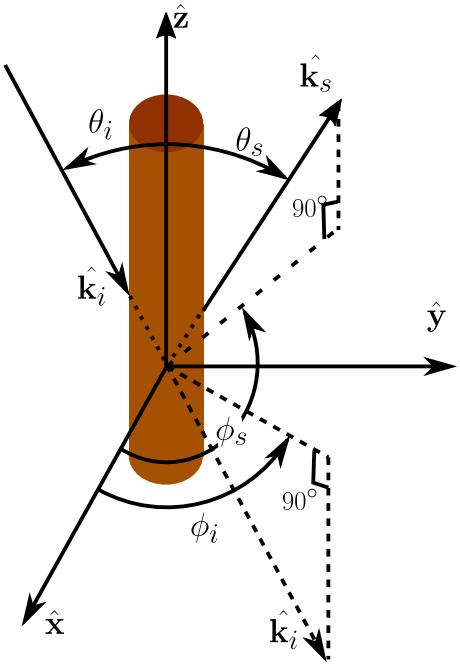

Figure 2.2: The angles and directions of the incident and scattered waves when the wave scatters off a cylinder.

2.5.1 Generalized Rayleigh-Gans estimation for a cylinder

Assuming an incoming plane wave ($\mathbf{E}^i$) represented by [11]

$$\mathbf{E}^i = (\hat{\mathbf{h}}\hat{\mathbf{h}} + \hat{\mathbf{v}}\hat{\mathbf{v}}) \cdot \mathbf{E}_0 e^{j\omega t - j\mathbf{k}_i\mathbf{R}} \tag{2.14}$$

where E_h^i is the electric field amplitude in the $\hat{\mathbf{h}}$ direction, E_v^i is the electric field amplitude in the $\hat{\mathbf{v}}$ direction, $\hat{\mathbf{R}}$ gives the wave propagation direction and the distance propagated and $\hat{\mathbf{h}}\hat{\mathbf{h}}$ represents a dyad. Assuming vectors and angles defined as in Figure 2.2 and that the cylinder stands in the $\hat{\mathbf{z}}$ direction, the vector $\hat{\mathbf{h}}$ and $\hat{\mathbf{v}}$ are defined by

$$\hat{\mathbf{h}} = \frac{\hat{\mathbf{z}} \times \hat{\mathbf{k}}_i}{|\hat{\mathbf{z}} \times \hat{\mathbf{k}}_i|} \tag{2.15a}$$

$$\hat{\mathbf{v}} = \hat{\mathbf{h}} \times \hat{\mathbf{k}}_i / k. \tag{2.15b}$$

The incoming and outgoing wave directions as can be seen in Figure 2.2 can be written as

$$\hat{\mathbf{k}}_i = \sin(\theta_i)(\hat{\mathbf{x}}\cos(\phi_i) + \hat{\mathbf{y}}\sin(\phi_i)) + \hat{\mathbf{z}}\cos\theta_i \tag{2.16a}$$

$$\hat{\mathbf{k}}_s = \sin(\theta_s)(\hat{\mathbf{x}}\cos(\phi_s) + \hat{\mathbf{y}}\sin(\phi_s)) + \hat{\mathbf{z}}\cos\theta_s. \tag{2.16b}$$

Under the assumption that one or two of the cylinders dimensions (length or diameter) is small in comparison to the wavelength, or $kD(\epsilon^{0.5}-1)\ll 1$, where D is the smallest dimension, the field inside the cylinder can be estimated as [9]

$$\alpha \cdot \mathbf{E}^i = \alpha \cdot (\hat{\mathbf{h}}\hat{\mathbf{h}} + \hat{\mathbf{v}}\hat{\mathbf{v}}) \cdot \mathbf{E}_0 e^{j\omega t - j\mathbf{k}_i\mathbf{R}} \tag{2.17}$$

where the polarizability tensor α is defined as [11]

$$\alpha = a_T\mathbf{I} + (a_N - a_T)\hat{\mathbf{z}}\hat{\mathbf{z}} \tag{2.18a}$$

$$a_T = \frac{1}{(\epsilon_r - 1)g_T + 1} \tag{2.18b}$$

$$a_N = \frac{1}{(\epsilon_r - 1)g_N + 1}. \tag{2.18c}$$

Here ϵ_r is the relative permittivity of the cylinder and g_T and g_N are demagnetizing factors. For cylinders that have a length much greater than the diameter, the demagnetizing factors and modifying function can be calculated as [11]

$$g_T = \frac{b}{2}\left(b + \frac{(b^2-1)}{2}\log\left(\frac{b-1}{b+1}\right)\right) \tag{2.19a}$$

$$g_N = -(b^2-1)\left(\frac{1}{2}b\log\left(\frac{b-1}{b+1}\right) + 1\right) \tag{2.19b}$$

$$b = \sqrt{1 - \left(\frac{2a}{h}\right)^2} \tag{2.19c}$$

$$\mu(\hat{\mathbf{k}}_s, \hat{\mathbf{k}}_i) = \frac{\sin[kh(\cos(\theta_i) + \cos(\theta_s))/2]}{kh(\cos(\theta_i) + \cos(\theta_s))/2} \tag{2.19d}$$

where a is the radius of the cylinder and h the length of the cylinder. The modifying function $\mu(\hat{\mathbf{k}}_s, \hat{\mathbf{k}}_i)$ was calculated under the assumptions that $2k_0a\sqrt{\epsilon_r} << 1$ and $a << h$. With this, the scattering parameters can be calculated according to [11]

$$S_{hh}(\hat{\mathbf{k}}_s, \hat{\mathbf{k}}_i) = \frac{k^2(\epsilon_r - 1)v_0}{4\pi}\cos(\phi_s - \phi_i)a_T\mu(\hat{\mathbf{k}}_s, \hat{\mathbf{k}}_i) \tag{2.20a}$$

$$S_{hv}(\hat{\mathbf{k}}_s, \hat{\mathbf{k}}_i) = \frac{k^2(\epsilon_r - 1)v_0}{4\pi}\cos(\theta_i)\sin(\phi_s - \phi_i)a_T\mu(\hat{\mathbf{k}}_s, \hat{\mathbf{k}}_i) \tag{2.20b}$$

$$S_{vh}(\hat{\mathbf{k}}_s, \hat{\mathbf{k}}_i) = \frac{k^2(\epsilon_r - 1)v_0}{4\pi}\cos(\theta_s)\sin(\phi_s - \phi_i)a_T\mu(\hat{\mathbf{k}}_s, \hat{\mathbf{k}}_i) \tag{2.20c}$$

$$S_{vv}(\hat{\mathbf{k}}_s, \hat{\mathbf{k}}_i) = \frac{k^2(\epsilon_r - 1)v_0}{4\pi}\left(a_N\sin(\theta_i)\sin(\theta_s) - a_T\cos(\theta_i)\cos(\theta_s)\cos(\phi_s - \phi_i)\right)\mu(\hat{\mathbf{k}}_s, \hat{\mathbf{k}}_i) \tag{2.20d}$$

where $v_0 = hr^2\pi$ is the volume of the cylinder.

Some limitations for the GRG approximation when used on cylinders with a length greater than its radius is that it only works when $ka << 1/\sqrt{\epsilon_r}$ and $h >$

$20a\sqrt{\epsilon_r}$ [12], [7]. These criteria means that the GRG method can not be used for too high frequencies or when the length is not sufficiently longer than the cylinder radius.

2.5.2 Truncated infinite cylinder approximation

The truncated infinite cylinder approximation works by estimating the field inside of an infinitely long cylinder and then truncating the cylinder so that it becomes of a chosen length. The electrical field inside the truncated infinite cylinder is assumed to be the same as it would have been for the infinite cylinder if it had not been truncated. The truncated infinite cylinder has a finite length h and a radius a. Assuming that the cylinder's long side stands in the $\hat{\mathbf{z}}$ direction the inner field can be written as [11], [10]

$$\mathbf{E}^i(r) = (E_{\rho h} + E_{\rho v})\hat{\rho} + (E_{\phi h} + E_{\phi v})\hat{\phi} + (E_{zh} + E_{zv})\hat{\mathbf{z}} \tag{2.21a}$$

$$E_{pq} = \sum_{n=-\infty}^{\infty} F_n \left(\frac{n\eta h_{nq} J_n(\lambda_i \rho)}{\lambda_i \rho} + j J_n'(\lambda_i \rho) e_{nq} \cos(\theta_i) \right) \frac{k}{\lambda_i} \tag{2.21b}$$

$$E_{\phi q} = \sum_{n=-\infty}^{\infty} F_n \left(-\frac{e_{nq} n J_n(\lambda_i \rho)}{\lambda_i \rho} \cos\theta_i + j J_n'(\lambda_i \rho) \eta h_{nq} \right) \frac{k}{\lambda_i} \tag{2.21c}$$

$$E_{zq} = \sum_{n=-\infty}^{\infty} F_n \left(e_{nq} J_n(\lambda_i \rho) \right) \tag{2.21d}$$

where q can be both v or h, $J_n()$ is a Bessel function with the derivative $J_n'()$, $\lambda_i = k\sqrt{\epsilon_r - \cos^2(\theta_i)}$ where ϵ_r is the cylinder's relative dielectric constant and

$$h_{nh} = \left(-\frac{J_n'(u)\epsilon_r}{J_n(u)u} + \frac{H_n'^{(2)}(v_i)}{H_n^{(2)}(v_i)v_i} \right) \frac{j\sin(\theta_i)}{R_n J_n(u)\eta} \tag{2.22a}$$

$$h_{nv} = n\cos(\theta_i) \left(-\frac{1}{u^2} + \frac{1}{v_i^2} \right) \frac{\sin(\theta_i)}{R_n J_n(u)\eta} \tag{2.22b}$$

$$e_{nh} = -\eta h_{nv} \tag{2.22c}$$

$$e_{nv} = \left(-\frac{J_n'(u)}{J_n(u)u} + \frac{H_n'^{(2)}(v_i)}{H_n^{(2)}(v_i)v_i} \right) \frac{j\sin(\theta_i)}{R_n J_n(u)} \tag{2.22d}$$

$$F_n = e^{jk_o z\cos(\theta_i) - jn\phi} E_0 j^{-n} \tag{2.22e}$$

$$u = a\lambda_i \tag{2.22f}$$

$$v_i = \sin(\theta_i) ak \tag{2.22g}$$

$$R_n = \left(\left[-\frac{J_n'(u)}{J_n(u)u} + \frac{H_n'^{(2)}(v_i)}{H_n^{(2)}(v_i)v_i} \right] \left[-\frac{\epsilon_r J_n'(u)}{J_n(u)u} + \frac{H_n'^{(2)}(v_i)}{H_n^{(2)}(v_i)v_i} \right] + \left[\frac{1}{v_i^2} - \frac{1}{u^2} \right] \cos^2(\theta_i) n^2 \right) \frac{H_n^{(2)}(v_i) v_i^2 \pi}{2} \tag{2.22h}$$

where $H_n^{(2)}$ is a Hankel functions with the derivative $H_n'^{(2)}$. The scattering matrix element can now be derived from combining the Helmholtz integral equation with

equation (2.21) and integrating. Using the directions described in Figure 2.2 the scattering matrix element can be written as [11]

$$S_{hh}(\hat{\mathbf{k}}_s, \hat{\mathbf{k}}_i) = 2\sum_{n=1}^{\infty}\left[(\eta h_{nh} B_n + j e_{nh}\cos(\theta_i) A_n)\right]\cos(\phi_s - \phi_i) \\ k^2 h(\epsilon_r - 1)\mu(\hat{\mathbf{k}}_s, \hat{\mathbf{k}}_i) + B_0 h_{0h}\eta k^2 h(\epsilon_r - 1)\mu(\hat{\mathbf{k}}_s, \hat{\mathbf{k}}_i) \tag{2.23a}$$

$$S_{hv}(\hat{\mathbf{k}}_s, \hat{\mathbf{k}}_i) = j2k^2 h(\epsilon_r - 1)\mu(\hat{\mathbf{k}}_s, \hat{\mathbf{k}}_i)\sum_{n=1}^{\infty}[(\eta h_{nv} B_n + \\ j e_{nv}\cos(\theta_i) A_n)\sin(n\phi_s - n\phi_i)] \tag{2.23b}$$

$$S_{vh}(\hat{\mathbf{k}}_s, \hat{\mathbf{k}}_i) = j2k^2 h(\epsilon_r - 1)\mu(\hat{\mathbf{k}}_s, \hat{\mathbf{k}}_i)\sum_{n=1}^{\infty}[((e_{nh}\cos(\theta_i) B_n - j\eta h_{nh} A_n) \\ \cos(\theta_s) - \sin(\theta_s) e_{nh} z_n)\sin(n\phi_s - n\phi_i)] \tag{2.23c}$$

$$S_{vv}(\hat{\mathbf{k}}_s, \hat{\mathbf{k}}_i) = k^2 h(\epsilon_r - 1)\mu(\hat{\mathbf{k}}_s, \hat{\mathbf{k}}_i)(e_{0v}(-\sin(\theta_s) z_0 + \cos(\theta_s)\cos(\theta_i) B_0) \\ +2\sum_{n=1}^{\infty}[((-j h_{nv} A_{nn}\eta + e_{nv}\cos(\theta_i) B_n)\cos(\theta_s) - \\ \sin(\theta_s) z_n e_{nh})\cos(n\phi_s - n\phi_i))]) \tag{2.23d}$$

where

$$\mu(\hat{\mathbf{k}}_s, \hat{\mathbf{k}}_i) = \frac{\sin[kh(\cos(\theta_i) + \cos(\theta_s))/2]}{kh(\cos(\theta_i) + \cos(\theta_s))/2} \tag{2.24a}$$

$$z_n = \frac{a^2}{u^2 - v_s^2}(u J_n(v_s) J_{n+1}(u) - v_s J_n(u) J_{n+1}(v_s)) \tag{2.24b}$$

$$v_s = ka\sin(\theta_s) \tag{2.24c}$$

$$A_n = k\frac{z_{n-1} - z_{n+1}}{2\lambda_i} \tag{2.24d}$$

$$B_n = k\frac{z_{n-1} + z_{n+1}}{2\lambda_i} \tag{2.24e}$$

For a more detailed description of these equations the paper [11] is recommended. A comparison between backscattering then using the truncated infinite cylinder- and the GRG approximation, for a cylinder with $a = 5$ cm, $h = 4$ m and $\epsilon_r = 9 + j4$, can be seen in Figure 2.3. The figure shows how the backscattering varies with frequency for both the GRG and the truncated infinite cylinder approximation for an angle of incidence $\theta_i = 40°$. Similar results can be found in [11], that develop this subject further.

The backscattering curves for the truncated infinite cylinder- and GRG approximation are very similar for the low frequencies but differs for the higher frequencies. The reason for this is the limitation $ka << 1/\sqrt{\epsilon_r}$, presented in Section 2.5.1, which is not true for the higher frequencies since $k = \omega\sqrt{\epsilon\mu}$ is increasing with the frequency.

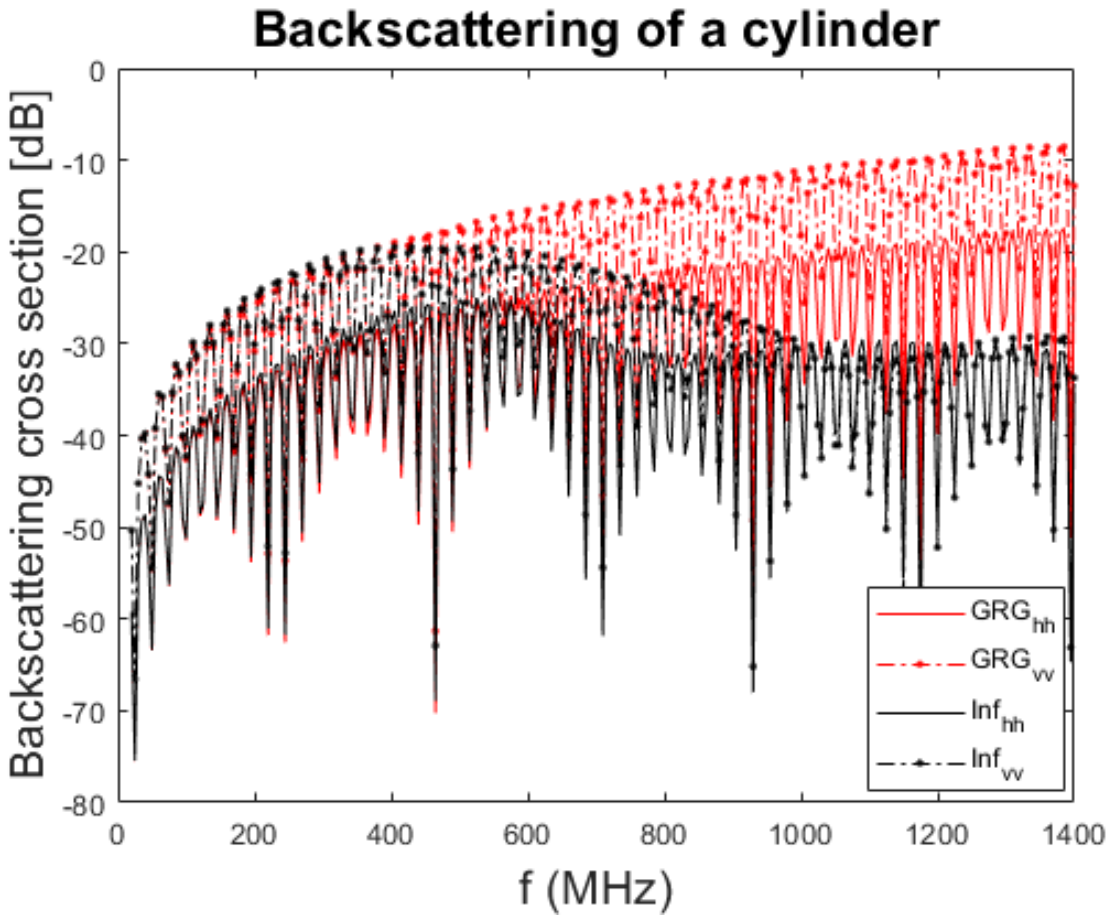

Figure 2.3: The backscattering cross section of a cylinder caused by an incidence wave with $\theta_i = 40°$ using the truncated infinite cylinder- and GRG approximation. The cylinder has $a = 5$ cm, $h = 4$ m and $\epsilon_r = 9 + j4$.

3

Method description

The goal of this thesis is to create an electromagnetic model of a forest area in between Skara and Skövde, perform computations, use the model on this area for the frequencies $20 - 1400$ MHz and evaluate whether the truncated infinite cylinder or GRG approximation are best to use. To accomplish this, data from SLU (Swedish University of Agricultural Sciences) collected by a research group that performed LIDAR measurement in the forest area were available. The measurement from the LIDAR contains point positions of objects that makes up the area surrounding the LIDAR see Figure 3.1. By using multiple LIDAR measurements from different positions, a forest area of 16541 m^2 that contained 748 treas was measured.

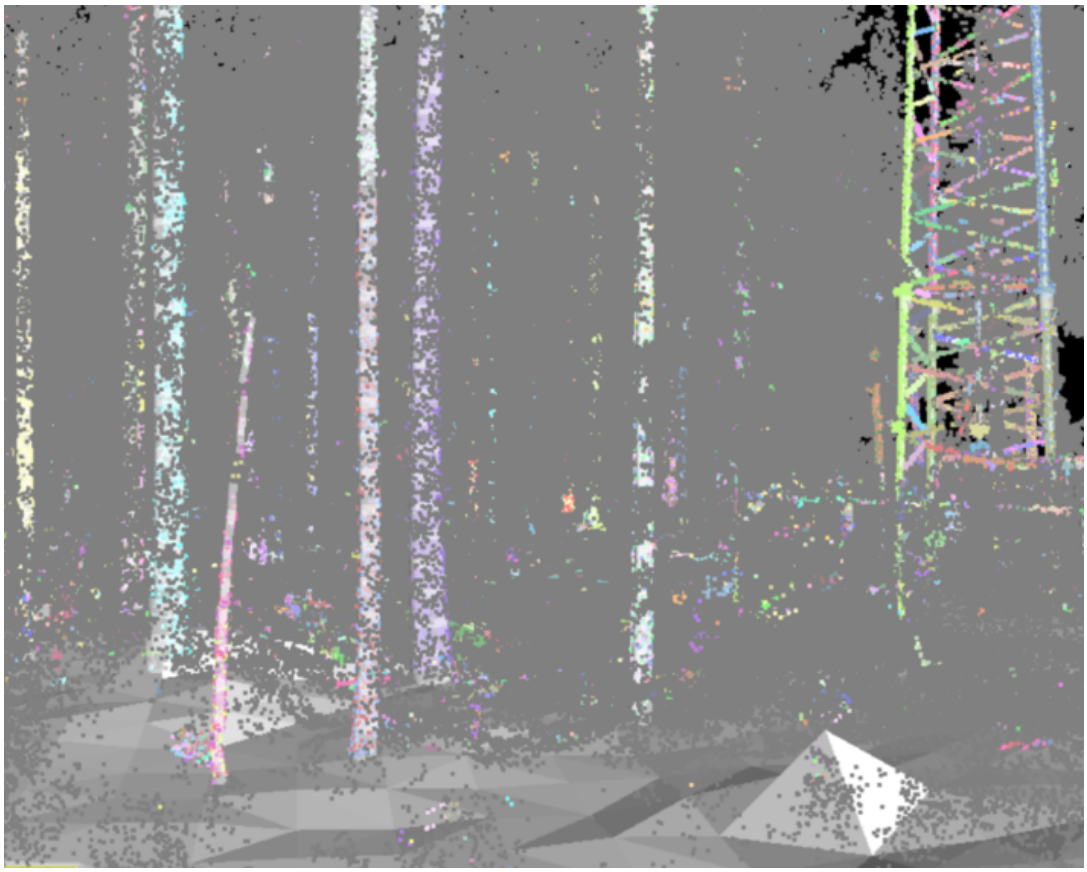

Figure 3.1: A figure created from the LIDAR measurements data where both trees, the lower part of an antenna tower and a small pyramid representing the LIDAR equipment can be seen.

To implement the project, the first task was to create a geometric model of the forest that contains the position and radii of cylinders, where a sum of cylinders put on top of each other represent an approximated tree. Secondly, a Matlab program was written which is capable of computing how an incident electromagnetic wave will propagate until it meets a tree trunk and how it is then scattered before propagating to a new location. This computation should be based on either the truncated infinite cylinder or GRG approximation. Thirdly, the Matlab program has to be adapted to work with the geometric forest model which has been developed and the attenuation caused by the forest will be added.

3.1 Geometric model of the forest

To create a geometric model of the forest, the LIDAR data in Figure 3.1 needed to be converted into usable Matlab data. The scattering matrix presented in equation (2.11) can only be calculated for certain object shapes and therefore the Matlab data needed to be transformed so that the Matlab model contains only these object shapes. Consequently, the LIDAR data of trees needed to be transformed so that the trees are described as a sum of cylinders and ground position data. The TLS data had already been processed to cylinders using the computer code developed by SLU [4]. Another code existed to derive the ground level in the local frame, the ground data was later used when calculating the scattering, and therefore data for the grounds position was easily obtained. However, the data derived from the existing code designed to derive cylinder data from the LIDAR data needed to be improved due to two reasons which can be seen in Figure 3.2. The first reason is that

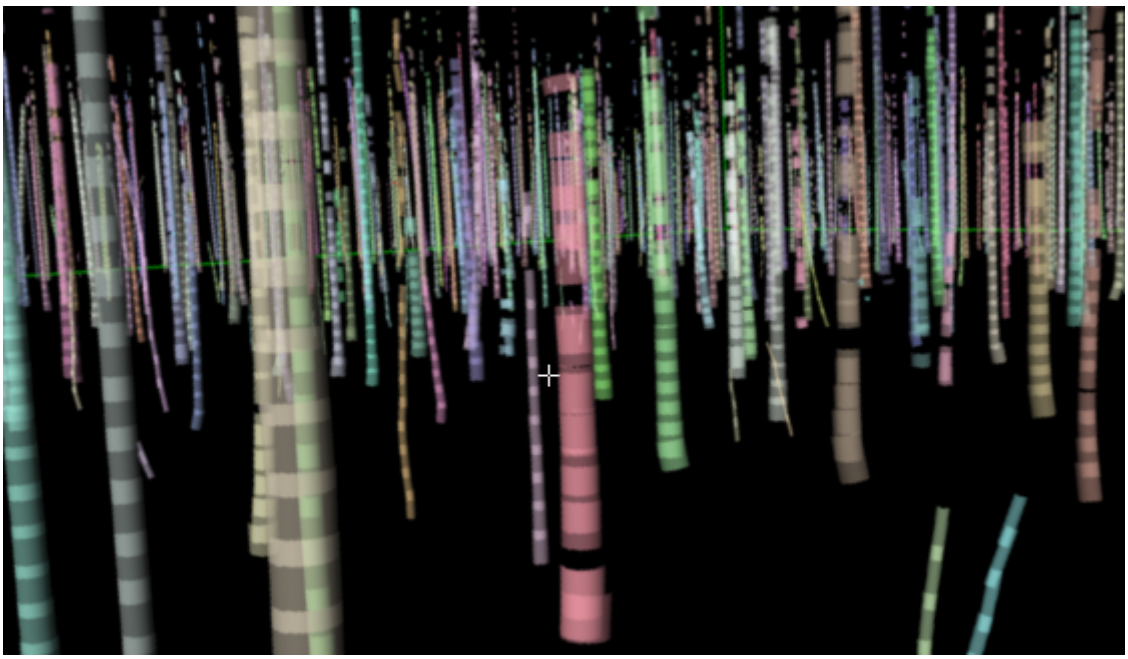

Figure 3.2: A figure created from the cylinder data derived by a computer code designed to derive cylinder data from LIDAR measurement data. The cylinders in the figure overlaps at some areas represented by a change in color intensity.

there are cases when the cylinders overlap with each other. If one does not remove this before the electromagnetic computation, the result will be incorrect. This is because the computation will calculate the scattering at the overlapping cylinders multiple times because of the fact that it looks as if two different cylinders occupy the same space. The second reason is that in some of the groups of cylinders that form a tree there are cylinders that are not connected to the other cylinders in the group. This will cause the computation to not calculate any scattering for the space between the cylinders that obviously should contain cylinders. Another reason, that can not be seen in the figure, is that the data provided gives the trees a total height, that in most cases is significantly higher than the highest cylinder position.

In this work, the resulting cylinder data was based on existing cylinder data from a previous work which was modified, so it was not based on the original LIDAR data. Since the existing cylinder data only contains information about the tree trunks and not tree branches, this is also be the case for the modified cylinder data.

3.1.1 Tree approximation using trucated cylinders

To create a more realistic tree model, the truncated cylinders can be used to approximate the tree using groups of cylinders without overlap or empty spaces between the cylinders. When creating this tree model, the constraint of the GRG approximation, presented in section 2.5.1, that $ka << 1/\sqrt{\epsilon_r}$ and $h > 20a\sqrt{\epsilon_r}$ should also be considered. Therefore this constraint was tried against a worst case scenario to see if the method could be used with the cylinder approximation or not. The frequency $f = 1400$ MHz, a tree radius bigger than 25 cm and $\epsilon_r = 9$ was used to test the constraints. This gives $ka = 7.34 > 1$ and $h > 15 = 20a\sqrt{\epsilon_r}$. Consequently, the GRG approximation will not be usable for the highest frequencies, and when it is used it will require extremely long cylinders with a length over 15 m. So long cylinders is too long to give a good tree approximation and the GRG method is therefore problematic to use. This is also the case even for lower frequencies. The truncated infinite cylinder approximation does not have the same constraint as the GRG approximation, and was therefore the method mainly used in this work. The groups of cylinders that were to approximate the trees was therefore not made to meet the GRG requirements. Instead, they were made to fit the truncated infinite cylinder approximation that does not have any problematic constraint.

When creating the geometrical model, problems can occur if the cylinder length is made too short or too long. If the cylinder length is too short the computational power needed in the computations will become greater than what is wanted and if the cylinder length is too long then the tree's shape will not be well represented. Bends and relative changes in radius occur faster for short and small trees and therefore the cylinder length for smaller tree segments should be shorter. The assumption that allowing the cylinder's length h to be a constant X times the radius a should, for some value on the variable X, give a reasonable representation of the tree shape. If nothing else is specified for a specific case X will be assumed to be 20 in this thesis. The results for some other values of X can be found in Figure 4.6.

The available cylinder data contains information about the cylinder's height, radius, position, the direction the cylinder is inclined, which cylinders that together

form a tree and the height of the trees. Using this, a relatively simple method to modify the cylinders so that the tree they formed would not have overlaps or open spaces between the cylinders was developed. We will assume the available cylinder data for a tree, that contains N cylinders with the radius a_n and where the position of the cylinder's bottom are $\mathbf{p}_{bn}$ and the position of the cylinders top are $\mathbf{p}_{tn}$ and where $n = 1, ..., N$. Here $n = 1$ represents the bottom cylinder and $n = N$ the top cylinder.

The method to create new cylinders, which has been developed, works by choosing a start point $p_s = \mathbf{p}_{b1}$ at the bottom of the first cylinder (which also is the foot of the tree) and checking if the distance to the top of the first cylinder $d_1 = ||\mathbf{p}_{t1} - \mathbf{p}_s|| > Xa_1$, where $||\mathbf{p}_{t1} - \mathbf{p}_s||$ is the Euclidian distance between $\mathbf{p}_{t1}$ and $\mathbf{p}_s$. This is due to the requirement on the length of the cylinder relative to its radius presented above. If $d_1 > Xa_1$, the first cylinder will start at $\mathbf{p}_s$ and ends at $\mathbf{p}_{t1}$. Otherwise, if $d_1 < Xa_1$, the method checks the distance from $\mathbf{p}_s$ to the top of the second cylinder ($\mathbf{p}_{t2}$). Now, if $d_2 = ||\mathbf{p}_{t2} - \mathbf{p}_s|| > X(a_1 + a_2)/2$ the first cylinder will start at $\mathbf{p}_s$ and ends at $\mathbf{p}_{t2}$. Otherwise, if $d_2 < X(a_1 + a_2)/2$ the process will be repeated and a third cylinder will be added. This goes on until $d_n = ||\mathbf{p}_{tn} - \mathbf{p}_s|| > Xa_{avg}$, where $a_{avg} = \sum_{i=1}^{n} a_i/n$. A cylinder that goes from $\mathbf{p}_s$ to $\mathbf{p}_{tn}$ is then created, with a radius a_{avg}, that is the average radius of the cylinders existing between $\mathbf{p}_s$ and $\mathbf{p}_{tn}$.

In the next step, a new starting point is chosen by setting $\mathbf{p}_s = \mathbf{p}_{tn}$ and the process will be repeated using the next cylinders until all cylinders have been used from $\mathbf{p}_{b1}$ to $\mathbf{p}_{tN}$. In the case when the last cylinder does not fulfill the length requirement ($||\mathbf{p}_{tN} - \mathbf{p}_s|| > Xa_{avg}$), the second-last cylinder will be made long enough to reach's $\mathbf{p}_{tN}$.

3.1.2 Tree approximation from the top cylinder to the tree top

Using the method described above, cylinder approximation was used to create a tree model. The cylinders starts at the tree root and goes to the tree's highest position according to the available cylinder data from SLU. However, the SLU data also gives the trees a total height, that in most cases, is significantly higher than the top cylinder position. This is due to the fact that the top of the trees have not been included in the cylinder data from SLU. This omission has so far not been treated, and the top of the tree needs to be included in the new cylinder model.

In the forest area studied, the trees that can be found are almost all Norway spruce whose shape, according to [5], can be described with the equations

$$D_i = Q \log(1 + (1 - i)\beta) \text{ for } 1 \geq i \geq i_v \tag{3.1a}$$

$$D_i = D_b - q \log(1 + \alpha i) \text{ for } i_v \geq i \geq 0, \tag{3.1b}$$

where i is the tree's relative height, D_i is the diameter at the height i, Q, q, α, β and D_b are constants and i_v is a height constant that determines which of the equations to be used when calculating D_i. The tree's relative height i is related to the tree's total height. The shape of the root of the trees are described by (3.1b) and is different from the rest of the tree and needs to be described by a different expression. This deviation will not be included in the cylinder model used in this

thesis because the cylinder data is available to a height much higher than i_v. The value of i_v is relatively small so the main part of the tree will be dealt with using (3.1a).

Using the cylinders approximated according to the method in Section 3.1.1, the least-squares method can be used to find a relation according to equation (3.1a). This relation relates the radius of the tree with the relative height and can then be used to estimate the cylinder's radius at a given height. New cylinders are created to describe the top of the tree and the radius of those cylinders are given by this relation. Then, by combining the cylinders approximated in Section 3.1.1 and the cylinders approximated using equation 3.1a an approximation of total tree is found. In Figure 3.3 the approximated trees, with the constant $X = 20$, in the forest area of interest can be seen as green lines together with a ground approximation.

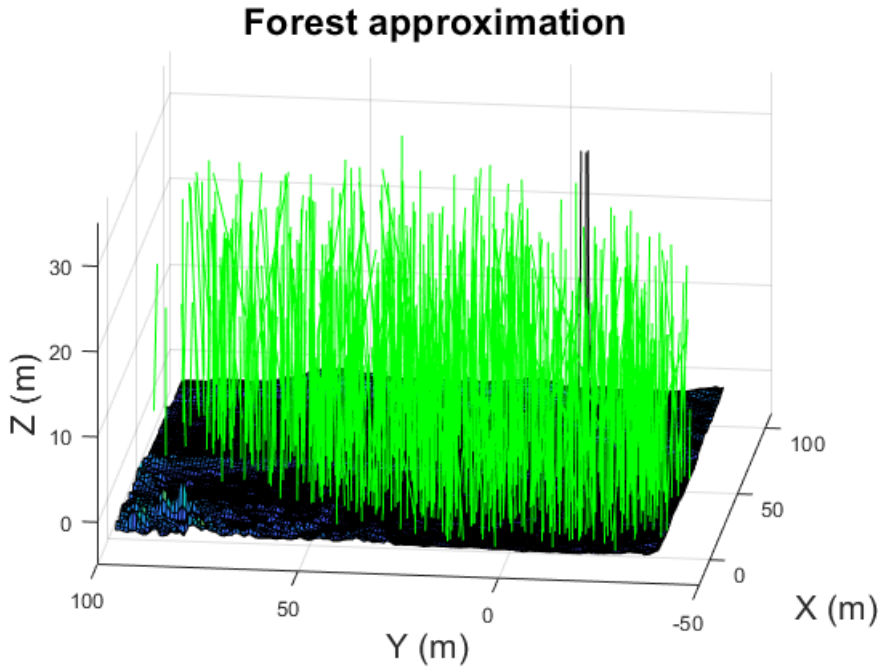

Figure 3.3: The approximated forest area plotted with trees as green lines together with the ground elevation. The three black lines sticking up above the rest is the antenna tower.

3.2 Computing the backscattering from a tree trunk

When a single tree, without branches, is standing on the ground and a parallel electromagnetic wave is incident, the backscattered wave will, among other things, depend on the ground reflections. The backscattered wave can be approximated as the sum of four different components, which are combinations of direct waves and ground scattered waves. This gives a total scattering matrix $\mathbf{S}$ given by

$$\mathbf{S} = \mathbf{S}_t e^{-jk2R_t} + \mathbf{S}_{tg} e^{-jk(R_t+R_{gt})} + \mathbf{S}_{gt} e^{-jk(R_t+R_{gt})} + \mathbf{S}_{gtg} e^{-jk2R_{gt}} \tag{3.2}$$

where $e^{-jk(R_t+R_{gt})}$ is a phase change caused by propagating a distance $R_t + R_{gt}$, where R_t is the distance between the wave's starting position and the tree and R_{gt} is the distance from the wave's starting position to the ground and then to the tree. For the scattering matrices S the index t represents the tree scattering, g represent the ground reflection and the combinations of g and t describes the way the wave propagates. Using this notation, the index gt represent that the incoming wave is reflected from the ground (g) to the tree (t), and then propagates directly back towards its starting position. Using this, the scattering matrix (3.2) can be calculated as [7]

$$\mathbf{S}_t = \mathbf{S}_0(\hat{\mathbf{k}}_{ta}, \hat{\mathbf{k}}_{at}) \tag{3.3a}$$

$$\mathbf{S}_{gt} = \mathbf{S}_0(\hat{\mathbf{k}}_{ta}, \hat{\mathbf{k}}_{gt})\Gamma(\hat{\mathbf{k}}_{gt}, \hat{\mathbf{k}}_{ag}) \tag{3.3b}$$

$$\mathbf{S}_{tg} = \Gamma(\hat{\mathbf{k}}_{ga}, \hat{\mathbf{k}}_{tg})\mathbf{S}_0(\hat{\mathbf{k}}_{tg}, \hat{\mathbf{k}}_{at}) \tag{3.3c}$$

$$\mathbf{S}_{gtg} = \Gamma(\hat{\mathbf{k}}_{ga}, \hat{\mathbf{k}}_{tg})\mathbf{S}_0(\hat{\mathbf{k}}_{tg}, \hat{\mathbf{k}}_{gt})\Gamma(\hat{\mathbf{k}}_{gt}, \hat{\mathbf{k}}_{ag}). \tag{3.3d}$$

where a represents the wave's starting position, t the tree, g the ground and index combinations like xz represent the direction from x to z. Further, $\mathbf{S}_0$ is the scattering matrix from the cylinder presented in section 2.5.2, $\hat{\mathbf{k}}_{at}$ is the incident direct wave direction and $\hat{\mathbf{k}}_{ta}$ is the direction of the backscattered direct wave, the directions of $\hat{\mathbf{k}}_{gt}$ is from the ground to the tree and $\hat{\mathbf{k}}_{tg}$ is from the tree to the ground and they can be calculated using equation (2.4) and Γ is the reflections matrix at the ground. It is assumed that the wave's starting position is placed so far away that all waves are parallel when they reach the tree.

Under the assumption that the tree stands straight up and that the ground has no slope, the scattering matrix $\mathbf{S}_0$ for an incoming wave with the frequency f can be calculated according to Section 2.5.2. The ground reflection matrix can be written as

$$\Gamma = \begin{bmatrix} \Gamma_{hh} & 0 \\ 0 & \Gamma_{vv} \end{bmatrix} \tag{3.4}$$

where Γ_{hh} and Γ_{vv} are calculated using (2.7) and (2.8).

3.2.1 Effect of ground backscattering

When the backscattering was computed, using equation (3.2), the ground was assumed to be perfectly planar without any change in permittivity. This is not a realistic scenario because in most real cases the ground will be rough and have changes in permittivity. The Rayleigh criterion says that a surface is even if the height variations is smaller than $\lambda/(32\cos(\theta_i))$ where θ_i is the incidence angel. Assuming that the ground roughness is less than 5 cm and the largest θ_i is 70° the criterion is true for frequency's below 550 MHz. This criterion is therefor true for the lower frequency's used in this project but not for the higher ones. In this thesis, the ground backscattering will be ignored when computing the total forest backscattering even if it have affect on the backscattering for the higher frequency's.

Since low frequency electromagnetic waves are used in this measurements, the wave will penetrate the ground surface. After penetrating the ground surface a wave may scatter off a rock or because of other objects that causes the permittivity to

change. The size of the objects and the used frequency will determine the scattering magnitude. Measurements of this backscattering process have been made in [7] and not found to be significant and it will therefore be ignored in the rest of this thesis.

3.2.2 Inclination of the ground plane and tree trunk

The inclination of the cylinder and ground plane will affect the scattering matrix. To be able to calculate the scattering matrix, the coordinate system needs to be changed to compensate for this inclination. A general formula for the normal to the plane ($\hat{\mathbf{n}}_g$) and the cylinder axis direction ($\hat{\mathbf{n}}_c$) can be written as

$$\hat{\mathbf{n}}_g = \cos(\phi_g)\sin(\theta_g)\hat{\mathbf{x}} + \sin(\phi_g)\sin(\theta_g)\hat{\mathbf{y}} + \cos(\theta_g)\hat{\mathbf{z}} \tag{3.5a}$$

$$\hat{\mathbf{n}}_c = \cos(\phi_c)\sin(\theta_c)\hat{\mathbf{x}} + \sin(\phi_c)\sin(\theta_c)\hat{\mathbf{y}} + \cos(\theta_c)\hat{\mathbf{z}} \tag{3.5b}$$

where θ_g is the angle between $\hat{\mathbf{n}}_g$ and $\hat{\mathbf{z}}$ and ϕ_g is the angle between $\hat{\mathbf{n}}_g$'s projection on the xy-plane and $\hat{\mathbf{x}}$. The angles θ_c and ϕ_c are defined in the same way but $\hat{\mathbf{n}}_g$ should be replaced by $\hat{\mathbf{n}}_c$.

To be able to calculate the scattering matrix for the tree and ground, the coordinate system can be changed to compensate for the inclination, and by doing so the computations will be simplified. This is done by choosing the $\hat{\mathbf{z}}'$ axis in the new coordinate system to be equal to $\hat{\mathbf{n}}_c$ or $\hat{\mathbf{n}}_g$, depending on which scattering matrix should be calculated. The other coordinate axes can then be chosen to be

$$\hat{\mathbf{x}}' = \frac{\hat{\mathbf{x}} - \hat{\mathbf{x}} \cdot \hat{\mathbf{z}}'}{|\hat{\mathbf{x}} - \hat{\mathbf{x}} \cdot \hat{\mathbf{z}}'|} \tag{3.6a}$$

$$\hat{\mathbf{y}}' = \hat{\mathbf{z}}' \times \hat{\mathbf{x}}' \tag{3.6b}$$

and a transformation matrix between the coordinate system can be written as

$$T = \begin{bmatrix} \hat{\mathbf{x}}' \cdot \hat{\mathbf{x}} & \hat{\mathbf{x}}' \cdot \hat{\mathbf{y}} & \hat{\mathbf{x}}' \cdot \hat{\mathbf{z}} \\ \hat{\mathbf{y}}' \cdot \hat{\mathbf{x}} & \hat{\mathbf{y}}' \cdot \hat{\mathbf{y}} & \hat{\mathbf{y}}' \cdot \hat{\mathbf{z}} \\ \hat{\mathbf{z}}' \cdot \hat{\mathbf{x}} & \hat{\mathbf{z}}' \cdot \hat{\mathbf{y}} & \hat{\mathbf{z}}' \cdot \hat{\mathbf{z}} \end{bmatrix} \tag{3.7a}$$

Now the direction of an incident wave ($\hat{\mathbf{k}}_i'$) and the scatted wave ($\hat{\mathbf{k}}_s'$) can be calculated in the new coordinate system as $\hat{\mathbf{k}}' = T\hat{\mathbf{k}}$. The horizontal ($\hat{\mathbf{h}}'$) and vertical ($\hat{\mathbf{v}}'$) directions for both $\hat{\mathbf{k}}_s'$ and $\hat{\mathbf{k}}_i'$ can be calculated with equation (2.15). Then the reflection matrix (Γ') and scattering matrix ($\mathbf{S}_0'$) can be calculated in the new coordinate system as before.

Now the scattering matrices need to be converted back to the original coordinate system before the total scattering matrix are calculated using equation (3.2) and (3.3). The conversion of the scattering matrix back to the original coordinate system can be done as [13], [14]

$$\begin{aligned} S_{pq} = {} & (\hat{\mathbf{p}}_s \cdot \hat{\mathbf{h}'}_s) S'_{0hh} (\hat{\mathbf{h}'}_i \cdot \hat{\mathbf{q}}_i) + (\hat{\mathbf{p}}_s \cdot \hat{\mathbf{v}'}_s) S'_{0vv} (\hat{\mathbf{v}'}_i \cdot \hat{\mathbf{q}}_i) \\ & + (\hat{\mathbf{p}}_s \cdot \hat{\mathbf{h}'}_s) S'_{0hv} (\hat{\mathbf{v}'}_i \cdot \hat{\mathbf{q}}_i) + (\hat{\mathbf{p}}_s \cdot \hat{\mathbf{v}'}_s) S'_{0vh} (\hat{\mathbf{h}'}_i \cdot \hat{\mathbf{q}}_i) \end{aligned} \tag{3.8}$$

where p ($\hat{\mathbf{p}}$) and q ($\hat{\mathbf{q}}$) can represent h ($\hat{\mathbf{h}}$) or v ($\hat{\mathbf{v}}$), respectively. The letter h is used to represent the horizontal polarization and the letter v the vertical polarization as in Section 2.2

3.2.3 Computation setups for one tree

There are many parameters and constants in the computation that can be varied and they are all affecting the result and cause changes to the backscattering. Some of these parameters have to do with how the tree is modelled, such as the tree size and the size of the cylinders that make up the tree. To perform computations of how the cylinder size and tree size affect the result, five tree models that can be seen in Figure 3.4, were created with equation (3.1a). The average height of the trees, approximated in the forest area in section 3.1, is approximately 19 m and this height is therefore chosen to be the height of the trees in Figure 3.4a.

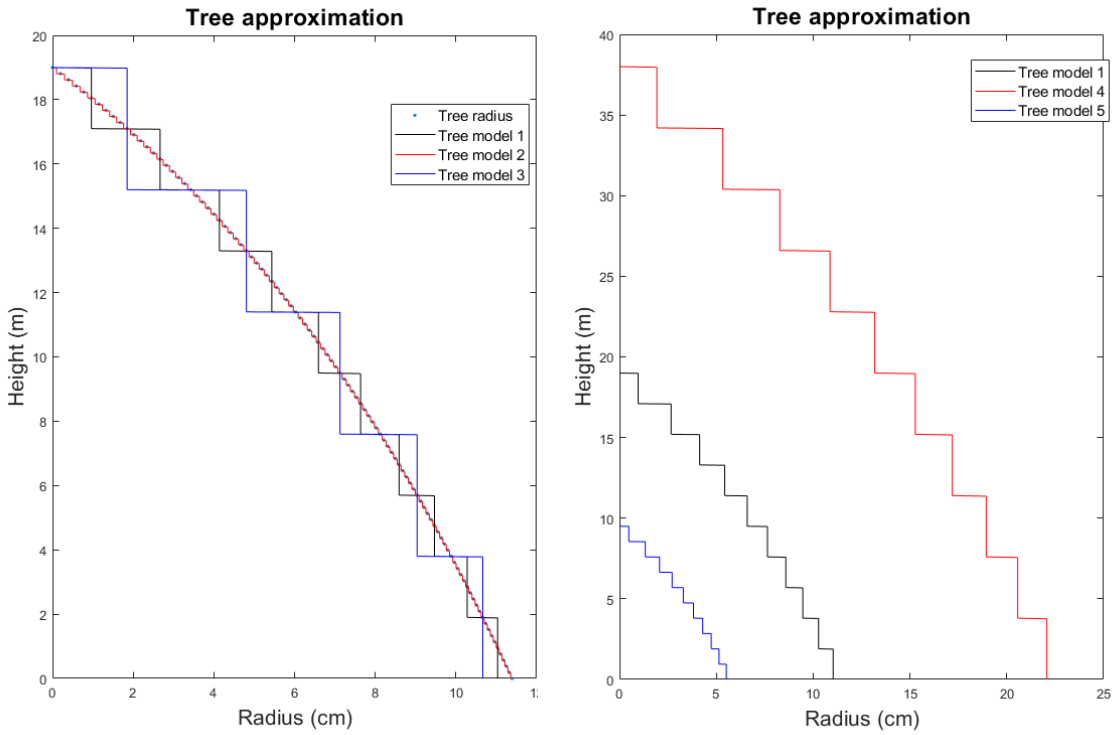

(a) (b)

Figure 3.4: Five, with equation (3.1a), approximated trees created by placing cylinders on top of each other. In (a), tree model 1 is made up of 10 cylinders while tree model 2 is made up of 100 cylinders and tree model 3 is made up of 5 cylinders. In (b) all tree models are made up of 10 cylinders but the radius and height have been doubled in model 4 and halved in model 5.

The three tree models are created with different cylinder sizes: tree model 1 is made up of 10 cylinders, tree model 2 is made up of 100 cylinders and tree model 3 is made up of 5 cylinders. In Figure 3.4b all tree models are made up of 10 cylinders but the radius and height have been doubled in model 4 and halved in model 5 in comparison to tree model 1. If nothing else is specified the tree model used in this rapport will always be tree model 1.

In reality, a tree also has branches that will affect the backscattering, but in this thesis the branches will be ignored if nothing else is mentioned. In the case that the

branches is mentioned, they will be approximated as cylinders. The backscattering from these cylinders will be calculated in the same way as the backscattering from the cylinders that makes up the tree. The assumption that a tree has 50 branches that are 4 m long and 1.5 cm thick will be used and they are assumed to be perpendicular to the tree stem axis. Assuming a vertical tree that has an axis in the $\hat{\mathbf{z}}$ direction the branches axis will be in xy-plane. The 50 branches are then placed on a random height on the tree with a random direction in the xy-plane.

Some parameters are in real life likely to vary because of environmental or weather conditions, like how the relative permittivity (ϵ_r) varies for the trees and the ground. In [6] more is explained about variation of ϵ_r for trees that in this thesis will have the value $\epsilon_r = 12.7 - j2.1$ if nothing else is specified. For moist soil, the permittivity can, based on real measurements, be calculated as [7]

$$\epsilon_{rground} = 11 - i\frac{\sigma_g}{2\pi f \epsilon_0} \tag{3.9}$$

where $\sigma_g = 0.001$ S/m. In this thesis, this value for the ground permittivity is used if nothing else is specified.

Other parameters that can be changed is the frequency, the direction $\hat{\mathbf{n}}_c(\theta_c, \phi_c)$ of the cylinders, the direction $\hat{\mathbf{n}}_g(\theta_g, \phi_g)$ of the ground normal and the incoming waves traveling direction $\hat{\mathbf{k}}_i = -\sin(\theta_i)\hat{\mathbf{x}} + \cos(\theta_i)\hat{\mathbf{z}})$. If noting else is specified the variables θ_g, ϕ_g, θ_c and ϕ_c will be assumed to be $0°$ and θ_i will be assumed to be $\theta_i = 60°$.

3.3 Forest simulation

The forest computation is similar to the computations for one tree since the computation for the forest computes the scattering of each tree individually and then sums them together. However, there are a few things that change because of the fact that the forest has a known antenna position. This changes how the RCS is calculated since equation (2.10) can no longer be used when the distance does not approach infinity. Instead equation (2.9) can be rewritten to calculate the RCS for one path of one cylinder by assuming the use of an omnidirectional antenna ($G_t = G_r = 1$). The radar cross section can in this case be written as

$$\frac{\sigma_{pq}}{R_t^2 R_r^2} = \frac{|E_p^r|^2}{|E_q^t|^2}\frac{(4\pi)^3}{\lambda^2} = |S_{pq}|^2 \frac{(4\pi)^3}{\lambda^2 R_t^2 R_r^2} \tag{3.10}$$

where E_q^t and E_p^r are the transmitted and received electrical fields respectively, R_t is the length that the wave travels from the antenna to the tree and R_r is the length that the wave travels from the tree to the antenna. If the wave is reflected at the ground between the antenna and tree the distance R is equal to the sum of the tree-to-ground distance and the ground-to-antenna distance.

Assuming that the forest model created earlier is built up of N cylinders, and taking the four paths in equation (3.2), there exist $N_{tot} = 4N$ different scattering paths. The number N represents the total number of cylinders in the forest. By assuming transmission of a continuous wave, a total backscattering coefficient (Ω)

can be calculated using the sum of the backscattering for all possible propagation paths as

$$\Omega = \frac{|E_p^r|^2}{|E_q^t|^2} = \frac{\sigma_{totpq}}{R^4}\frac{\lambda^2}{(4\pi)^3} \tag{3.11a}$$

$$\frac{\sigma_{totpq}}{R^4} = \frac{(4\pi)^3}{\lambda^2}\left|\sum_{n=1}^{N_{tot}} \frac{S_{npq}e^{-jk(R_{tn}+R_{rn})}}{R_{tn}R_{rn}}\right|^2 \tag{3.11b}$$

where different values of n represent the different cylinder reflection paths and $e^{-jk(R_{tn}+R_{rn})}$ is the phase shift caused by the different traveling distances for the different paths. The factor σ_{totpq} can be interpreted as the forest's total radar cross section seen from the antennas direction and distance R from some defined center of the forest.

In this thesis, both a Born approximation and a distorted Born approximation of the forest backscattering will be used. In the Born approximation, the branches' attenuation and backscattering will be ignored while in the distorted Born approximation only the branches' backscattering will be ignored. In the distorted Born approximation, the attenuation caused by branches and trunks when the wave propagates trough the forest, will be considered when calculating the scattering matrix. The attenuation matrix ($\mathbf{A}$) can be calculated as in Appendix A.1 (see Figure A.1), and needs to be incorporated into equation (3.3). Hence, equation (3.3) will become

$$\mathbf{S}_t = \mathbf{A}_{ta}\mathbf{S}_0(\hat{\mathbf{k}}_{ta}, \hat{\mathbf{k}}_{at})\mathbf{A}_{at} \tag{3.12a}$$

$$\mathbf{S}_{gt} = \mathbf{A}_{ta}\mathbf{S}_0(\hat{\mathbf{k}}_{ta}, \hat{\mathbf{k}}_{tg})\mathbf{A}_{tg}\Gamma(\hat{\mathbf{k}}_{tg}, \hat{\mathbf{k}}_{ag})\mathbf{A}_{ag} \tag{3.12b}$$

$$\mathbf{S}_{tg} = \mathbf{A}_{ga}\Gamma(\hat{\mathbf{k}}_{ga}, \hat{\mathbf{k}}_{tg})\mathbf{A}_{tg}\mathbf{S}_0(\hat{\mathbf{k}}_{tg}, \hat{\mathbf{k}}_{at})\mathbf{A}_{at} \tag{3.12c}$$

$$\mathbf{S}_{gtg} = \mathbf{A}_{ga}\Gamma(\hat{\mathbf{k}}_{ga}, \hat{\mathbf{k}}_{tg})\mathbf{A}_{tg}\mathbf{S}_0(\hat{\mathbf{k}}_{tg}, \hat{\mathbf{k}}_{gt})\mathbf{A}_{gt}\Gamma(\hat{\mathbf{k}}_{tg}, \hat{\mathbf{k}}_{ag})\mathbf{A}_{ag} \tag{3.12d}$$

where the indices are explained in equation (3.3).

3.3.1 Ground approximation

When calculating the reflections at the ground, information about the the inclination and elevation of the ground is necessary. In the case when the tree trunk was approximated with cylinders, this was assumed to be known. This information is also included in the forest data, but the ground and it's inclination are varying as can be seen in Figure 3.3. To handle this, the ground's elevation and inclination for each reflection will be calculated with the least-squares method. This is done while using data from a small area around an approximated reflection point p_{aprox}.

Using the elevation data from the ground in Figure 3.3 an average elevation E_{avg} can be calculated. Using the assumption that the ground has an elevation E_{avg} and a normal in the $\hat{\mathbf{z}}$ direction, p_{aprox} can be calculated. Then, by using all the elevations data from the area within 2 m of p_{aprox}, the elevation of the ground plane can be estimated. This is done using the least-squares method to minimize the elevation error of the approximated elevation level compared to the elevation data. Using the approximated ground elevation, the slope the reflection matrix (Γ)

can be calculated as usual. The average variance when comparing the real elevation to the estimated elevation, inside a 2 m distance from a grid of estimated reflection points, was 4.6 cm. A plot over how the variance changes depending on the position of the estimated reflection point can be seen in Figure 3.5.

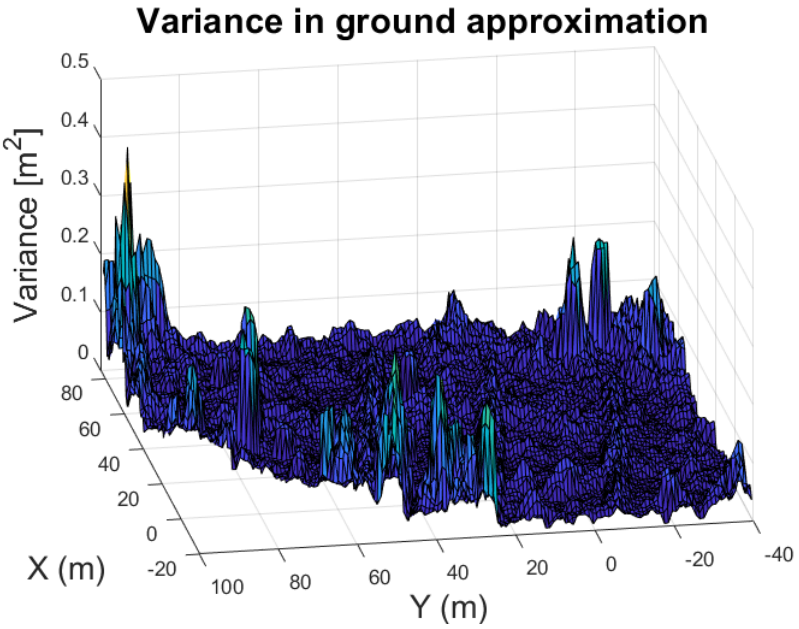

Figure 3.5: The variance between the elevation of the estimated ground plane and the real ground plane. The reason a corner is missing, when compared to Figure 3.3, is because there are no trees in that corner and those data are therefore omitted.

3.3.2 Forest computation setup

The computation setup is best described with Figure 3.3 that, as earlier described, was created from LIDAR data. The different parameters that can be changed, have the same values as in the computation setups for one tree if nothing else is specified. However, the forest computation has three parameters that can be varied that was not used in the simulation setups for one tree. The first one is X, which was introduced in Section 3.1.1, that describes how the approximated cylinder's length should compare to the cylinder radius. The second parameter that can be varied is the antenna position at the top of the antenna tower, that can be seen in Figure 3.3. In reality, the antenna position is stationary, but the exact antenna position is not known and the result of moving the antenna by small distances could produce similar effects as when the trees move with the wind. Another thing that will be tried is a comparison between measuring the backscattering with and without branch attenuation. If noting else is specified the variable X will be assumed to be 20 and the antenna position will be assumed to be $(79.5, -8, 50)$ (see Figure 3.3).

4

Results

In this chapter, the results from the computation of the backscattering from a single tree trunk and the backscattering from a complete forest will be presented. First, the computation of the backscattering from a single tree trunk, described in Section 3.2, will be presented. These results will be helpful in the interpretation of the result of the backscattering from the forest. The result for the forest backscattering will then be presented using the setup described in Sections 3.1 and 3.3

4.1 Backscattering from a single tree trunk

In this section, the results of the backscattering from a plane wave incident on a single tree trunk standing on a ground is presented. There are many parameters in the model that can be varied, allowing for different results for a wide variety of real world situations. For a more detailed explanation, see Section 3.2.3.

First, the result from computations using the different tree models, presented in Section 3.2.3, will be presented. Then, the effect of changing the inclination angles (θ_g, ϕ_g, θ_c and ϕ_c) of the tree and the ground will be presented. Finally, the RCS for the tree models with and without branches will be compared.

4.1.1 Backscattering for trees of different sizes

How the backscattering varies depending on tree size is important to know when trying to measure the biomass in a forest area. When performing forest measurements it would be good to have clear and simple relations between the measured backscattering and the forest properties. Therefore in an ideal case, the backscattering should be proportional to the tree volume or tree mass for all frequencies, but as can be seen in Figure 4.1, this is not the case. Figure 4.1 shows the radar cross section (RCS) for an incident and reflected horizontal polarization of the wave (σ_{hh}) and and for the corresponding vertical polarization (σ_{vv}), calculated according to equation (2.13). The results are shown for tree models 1,4 and 5, which are described in Section 3.2.3.

Every cylinder that makes up tree model 4 has a radius and length twice that of the corresponding cylinders in tree model 1 and every cylinder that makes up tree model 5 has a radius and length half that of the corresponding cylinders in tree model 1. This means that tree model 4 has a volume 8 times that of tree model 1 which has a volume 8 times that of tree model 5. Using the specific setup described

in Figure 4.1, σ_{vh} and σ_{hv} will become zero because neither the ground nor the tree changes polarization of the wave.

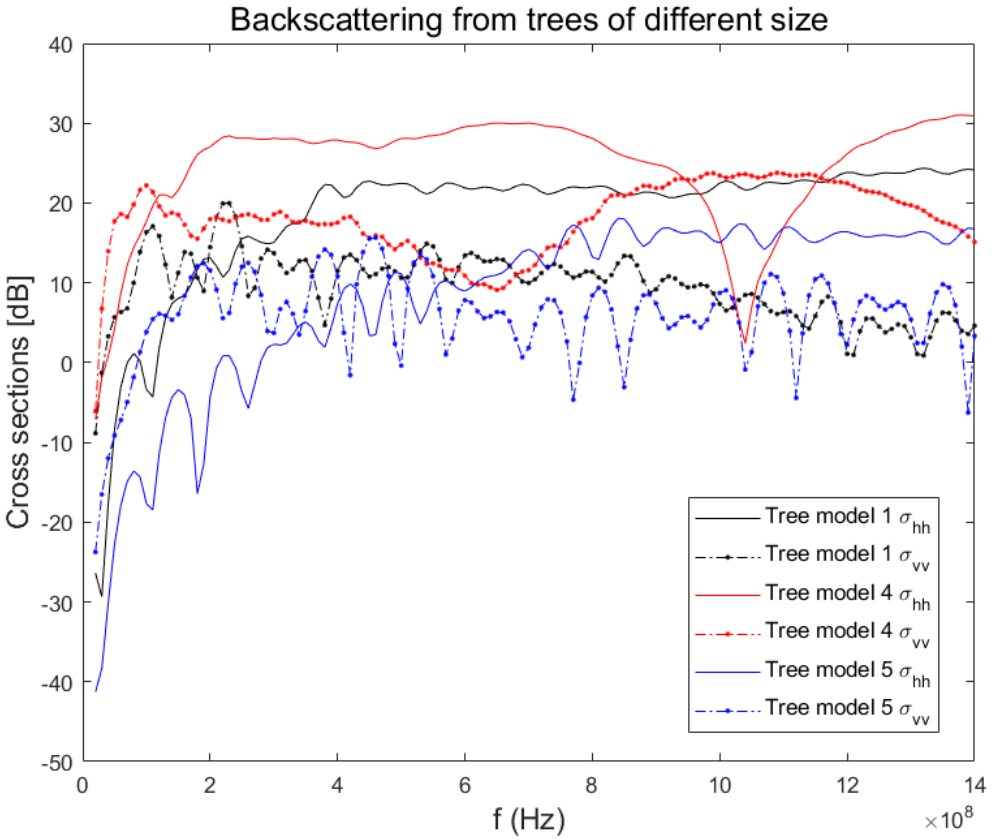

Figure 4.1: Using the tree model 1,4 and 5, described in Section 3.2.3, σ_{hh} and σ_{vv} have been plotted against the frequency. Tree model 4 has a volume eight times that of tree model 1 which has a volume eight times that of tree model 5. The figure was created using a dielectric horizontal ground plane $\theta_g = 0°$ $\phi_g = 0°$, $\theta_c = 0°$, $\phi_c = 0°$, $\theta_i = 60°$ and $\epsilon_r = 12.7 - j2.1$

While looking at the σ_{hh} in Figure 4.1, it is apparent that the larger tree models have a larger radar cross section (σ). The magnitude difference between the different σ_{hh} varies over the frequency band and seems to be greater for the lower frequencies (20-400 MHz). For low frequency's, when the wave is Rayeleigh scattered, the backscattering should be proportional to the square off the volume which is in line with the results of the computations. The amplitude variations for frequencies above 400 MHz, are for σ_{hh} when comparing tree model 1 and 4 or when comparing tree model 1 and 5 mostly between 4 and 12 dB. On average, the difference is less than 9 dB and this means that increasing the tree's volume eight times will not necessarily increase the backscattering by eight times. The reason for this can be the fact that the wave scattering happens partially at the tree's surface. This may mean that the surface area of the tree determines the scattering, but the amplitude difference of the different σ_{hh} is usually greater than 6 dB. It therefore seems like σ_{hh} does not scale linearly with the tree's surface area either. It may be so that some combination

of the tree surface area and volume determines the amplitude of σ_{hh}. However, the result shows a connection between the tree size and σ_{hh} which implies that it is feasible to use σ_{hh} to estimate the biomass.

When the wavelength of an incident wave is much longer than the size of it's scattering object, the wave will be Rayleigh scattered. This can be used to explain the abnormality for tree model 4, where the amplitude diminishes for σ_{hh} and increases for σ_{vv} around the frequency 1 GHz. This is because at this frequency (1 GHz) the wavelength is approximately the same as the tree's diameter. This means that the waves will not be Rayeleigh scattered and when the frequency is increased further the scattering process will be transformed into optical scattering. Optical scattering occurs when the objects size is much greater than the wavelength. The effect is caused by the wavelength becoming close to the cylinder diameter. Attempts were made, where the frequency was increased to produce corresponding effects for tree model 1 and 5. The effects were found for model 1 at frequencies around 2 GHz and for model 5 at 4 GHz.

The σ_{vv}, like the σ_{hh}, shows that the backscattering from the larger trees are greater than the backscattering from the smaller trees. But the σ_{vv} are fluctuating more than the σ_{hh}. This results in that σ_{vv} for some frequencies are greater for a small tree than for a large tree. Because of the greater stability and a more stable relation between σ and the tree size, σ_{hh} seems to be more appropriate to use when measuring the backscattering to estimate the tree size than σ_{vv} for this setup. However, changing the parameters, like ϵ_r, changes the size of the fluctuations for σ_{hh} and σ_{vv} so this is not always the case.

4.1.2 Backscattering using different cylinder sizes

The backscattering variations, depending on the cylinder size, can be used to determine the necessary cylinder size to be used in the forest model. This is because, if the backscattering from the longer cylinders differs from the backscattering from the shorter cylinders it may be due to approximation errors. Figure 4.2 shows σ_{hh} and σ_{vv} calculated according to equation (2.13), for tree model 1,2 and 3 described in Section 3.2.3. All three tree models are of the same size but with the difference that tree model 1 is made up of 10 cylinders, tree model 2 is made up of 100 cylinders and tree model 3 is made up of only 5 cylinders. For the specific setup described in Figure 4.2, σ_{vh} and σ_{hv} will become zero.

While looking at σ_{hh} in Figure 4.2 it is apparent that the curve created using tree model 2 fluctuate more than the other curves for frequencies above 400 MHz. This is because tree model 2 is using more cylinders than the other tree models which allows for more variations in the backscattering. The fluctuation of σ_{hh} for tree model 2 is however approximately centred around the other tree models value of σ_{hh}. This implies, that even though the σ_{hh} value fluctuates differently depending on the number of cylinders in the tree model, the value is still following the same general curve. The great fluctuations for figure 4.2 is not physical and may be caused by neglected interactions between cylinders. If one only is interested in approximate σ_{hh} for a frequency interval, the estimation of σ_{hh} using tree models with 5 to 10 cylinders are better than using tree models with many more cylinders.

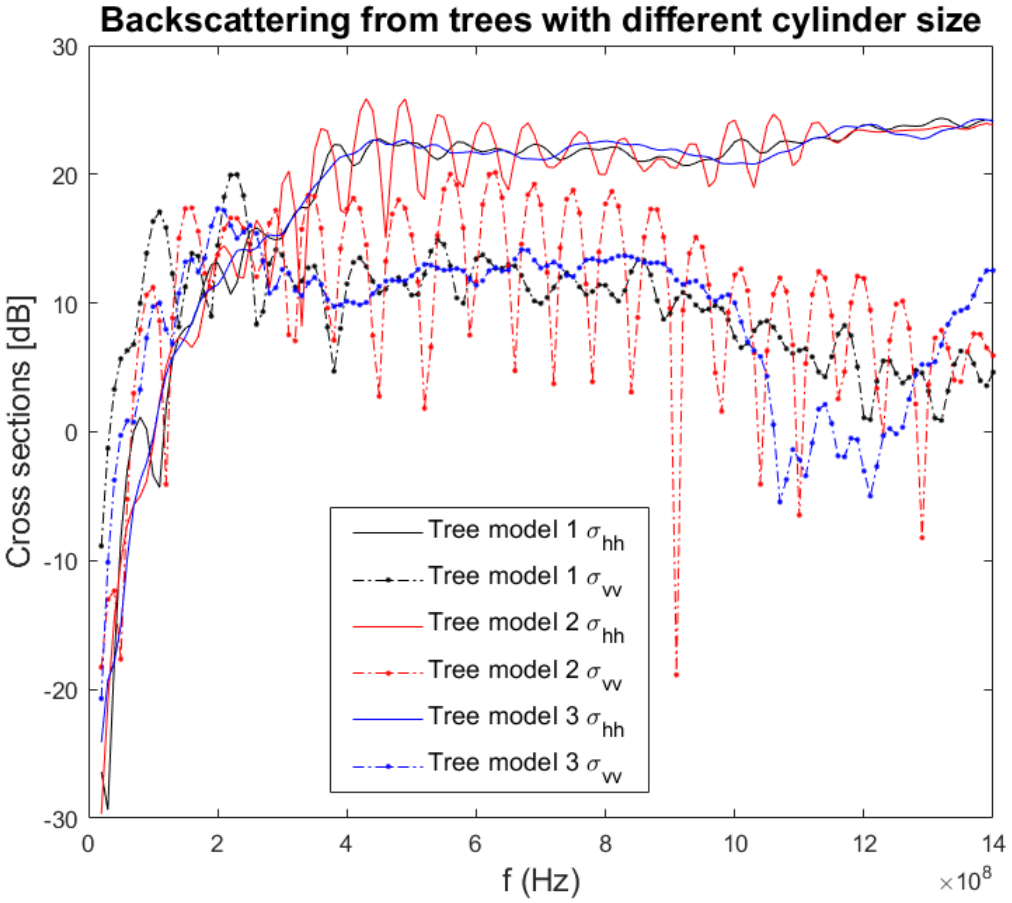

Figure 4.2: The values of σ_{hh} and σ_{vv} are plotted against the frequency for tree model 1,2 and 3 described in Section 3.2.3, Tree model 2 is made up of ten times as many cylinders as tree model 1 that is made up of twice as many cylinders as tree model 3. The trees are of the same size in all models. The figure was created using a dielectric horizontal ground plane $\theta_g = 0°$, $\phi_g = 0°$, $\theta_c = 0°$, $\phi_c = 0°$, $\theta_i = 60°$ and $\epsilon_r = 12.7 - j2.1$

Similar observations can be made for σ_{vv}, with the difference that the fluctuations are greater even for tree model 1, where the σ_{vv} value can be seen fluctuating.

The average amplitude of σ_{hh} and σ_{vv} does not seem to have any obvious dependence on the number of cylinders used in the simulation. This means that it might be possible to only use a few cylinders when simulating the average value of σ_{hh} or σ_{vv}. This is advantageous because computations using many cylinders for each tree would take a lot more computing power than computations using only a few cylinders for each tree.

For the frequencies lower than 400 MHz an obvious increase of σ_{hh} and σ_{vv} can be seen as the frequency increases. Also for the lower frequencies the values computed using many cylinders in the tree model can be seen fluctuating more than the values computed using fewer cylinders in the tree model.

The value of σ_{hh} in Figure 4.2 seems to be more stable than the value of σ_{vv} when the number of cylinders in the tree model changes. This can be seen in that

the σ_{hh} changes very little for the frequencies above 400 MHz in comparison to σ_{vv}. An abnormality can also be seen in the σ_{vv} curve for tree model 3 in the frequency interval $1 - 1.2$ GHz where the σ_{vv} value drops significantly.

4.1.3 Backscattering for different ground slopes

Knowing how the backscattering varies depending on the ground slope (θ_g, ϕ_g) is advantageous when performing backscattering measurements on hills or sloping grounds. Figure 4.3 shows how the computed σ varies for tree model 1, described in Section 3.2.3, when θ_g and ϕ_g varies. A similar figure can be found in [7].

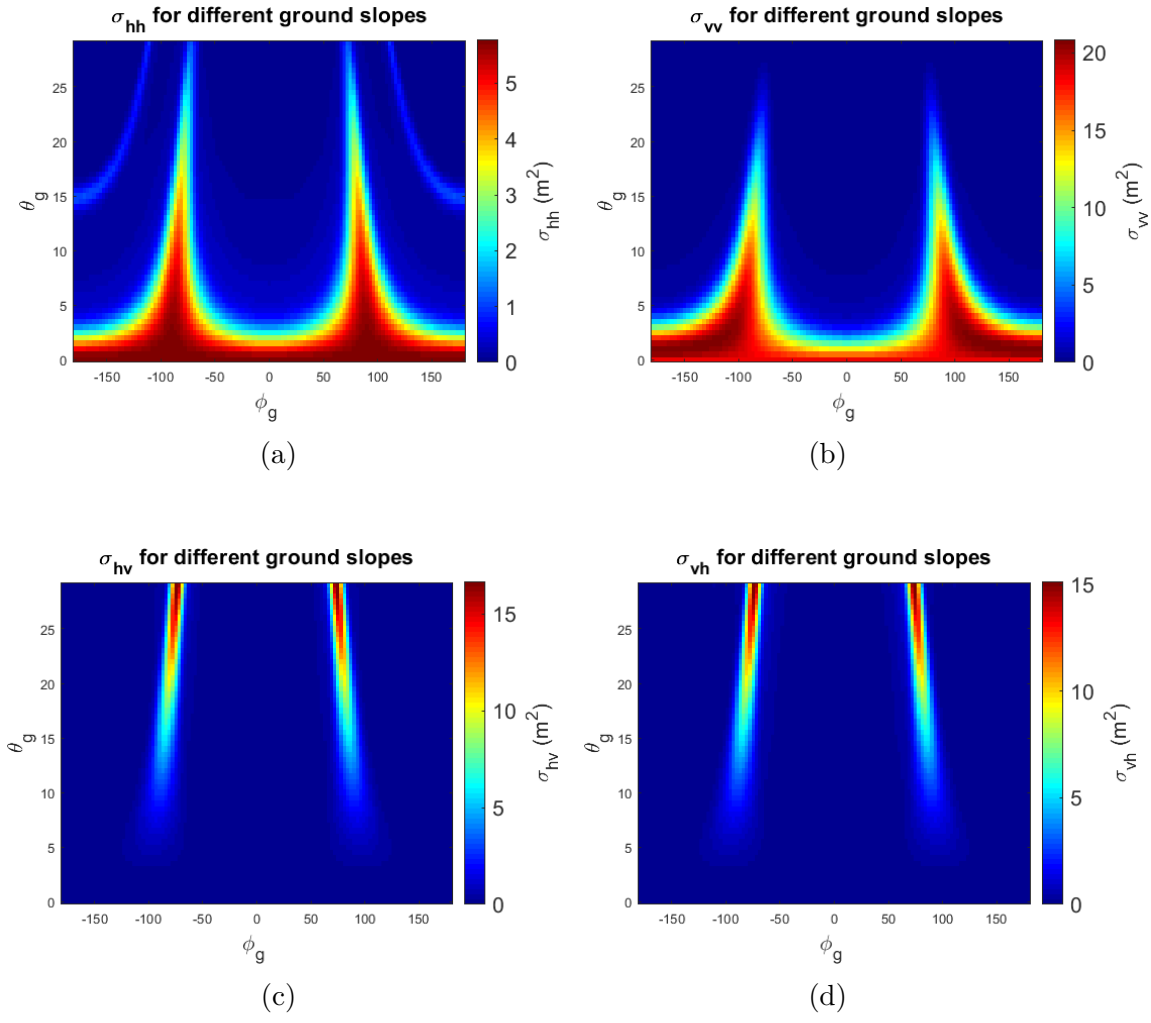

Figure 4.3: The RCS (σ) for a single tree trunk standing on a ground plane with varying inclination. Figure a, b, c and d shows how σ_{hh}, σ_{vv}, σ_{hv} and σ_{vh} vary with different θ_g and ϕ_g. The figures were computed using tree model 1 described in section 3.2.3 with $\theta_c = 0°$, $\phi_c = 0°$, $\theta_i = 60°$, $\epsilon_r = 12.7 - j2.1$ and the frequency $f = 150$ MHz.

The values of σ_{hh} and σ_{vv} in Figure 4.3, can be seen to rapidly decrease for $\phi_g = 0°$ and $\phi_g = 180°$ when θ_g increase. But, when $\phi_g = \pm 90°$ the magnitude of σ_{hh} and σ_{vv} will not decrease as rapidly when θ_g increases. This has to do with

that the largest contributor to σ is the ground-trunk ($\mathbf{S}_{gt}$) and trunk-ground ($\mathbf{S}_{tg}$) scattering, described in equation (3.3). When $\theta_g = 0°$, the backscattering for $\mathbf{S}_{tg}$ and $\mathbf{S}_{gt}$ occur, so that for the tree the reflected and incident wave direction have the same angular distance to the tress surface normal. When this changes, as it does when the ground's inclination in the waves traveling direction changes, σ_{hh} and σ_{vv} will decrease. Since the inclination in the wave's traveling direction changes faster the closer ϕ_g is to 0° or 180°, σ_{hh} and σ_{vv} will decrease faster for $\phi_g = 0°$ and $\phi_g = 180°$ when θ_g is increased. Similarly, the inclination in the waves traveling direction does not changes when ϕ_g is ±90° and therefore σ_{hh} and σ_{vv} will not decrease so fast for $\phi_g = \pm 90$ when θ_g is increased.

In Figure 4.3a, at $\phi_g = 180°$ and $\theta_g = 15°$, one can see that the σ_{hh} value has a local peak compared to higher and lower values of θ_g. This peak shifts towards larger θ_g-values as ϕ_g becomes larger or smaller. The peak is due to the ground-tree-ground scattering ($\mathbf{S}_{gtg}$), and occurs when the from the ground reflected wave traveling direction is orthogonal to the tree trunk giving $\hat{\mathbf{k}}_{gt} = -\hat{\mathbf{k}}_{tg}$.

The cross-polarized radar cross sections, σ_{hv} and σ_{vh}, in Figure 4.3 can bee seen to be zero when $\phi_g = 180°$, $\phi_g = 0°$ or $\theta_g = 0°$. This is because neither the tree scattering matrix nor the ground reflection matrix contributes to any polarization changes for thees angles. But then $\phi_g = \pm 90°$, the ground reflection matrix after the coordinate system changes, described in equation (3.8), will have cross-polarized components. Even the tree scattering matrix will then have cross-polarized components that are not zero, this is due to $\phi_s \neq \phi_i$, described in Figure 2.2.

The magnitude of σ_{hv} and σ_{vh}, when they attain their maximum value, are larger than the magnitude of σ_{hh}. This means that the backscattering from σ_{hv} and σ_{vh} can be significant at hills due to the ground inclination.

4.1.4 Backscattering for different tree inclinations

Knowing how the backscattering varies depending on the inclination of the tree (θ_c, ϕ_c) can be useful then performing backscattering measurements on a forest. Figure 4.4 shows how the computed σ varies for tree model 1, described in Section 3.2.3, when θ_c and ϕ_c is varied.

There are many similarities in Figure 4.4 and 4.3 that can bee seen if comparing the figures. One such similarity is how the values of σ_{hh} and σ_{vv} can be seen to rapidly decrease for $\phi_c = 0°$ or $\phi_c = 180°$, when θ_c is increased. However when $\phi_c = \pm 90°$, the magnitude of σ_{hh} and σ_{vv} will not decrease as fast. The reason for this is due to the ground-trunk ($\mathbf{S}_{gt}$) and trunk-ground ($\mathbf{S}_{tg}$) scattering described in equation (3.3). When the inclination is changed, the reflected and incident waves' direction will not have the same angular distance to the trees surface normal causing σ_{hh} and σ_{vv} to decrease. This happens faster for angles close to $\phi_g = 0°$ or $\phi_g = 180°$ and slower fore angles close to $\phi_c = \pm 90°$.

There are some things in Figure 4.4 that can not be seen in Figure 4.3, like how σ_{hh} has a barely visible peak at $\theta_c = 30°$ when $\phi_c = \pm 180°$ and θ_c is varied. As ϕ_c changes, the peaks will change towards larger θ_c values. This is caused by the incident and reflected wave directions for $\mathbf{S}_t$, presented in equation (3.3), being both normal to the tree inclination or $\hat{\mathbf{k}}_{ta} = -\hat{\mathbf{k}}_{ta}$. When ϕ_c or θ_c then changes the

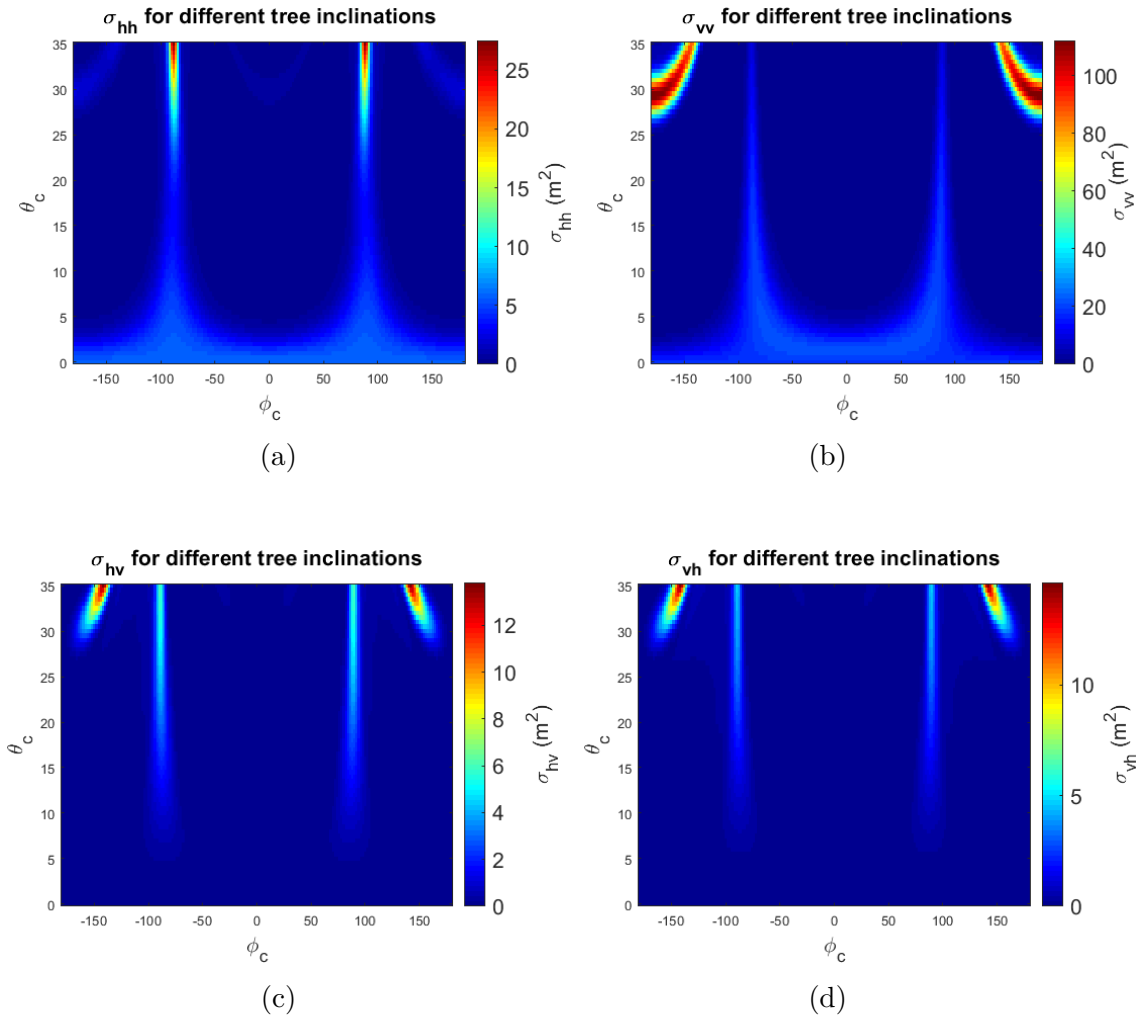

Figure 4.4: The RCS (σ) for a single tree trunk with varying inclinations to a ground plane without any slope. Figure a, b, c and d shows how σ_{hh}, σ_{vv}, σ_{hv} and σ_{vh} varies with different θ_c and ϕ_c. The figures where created using tree model 1, described in section 3.2.3, with $\theta_g = 0°$, $\phi_g = 0°$, $\theta_i = 60°$, $\epsilon_r = 12.7 - j2.1$ and $f = 150$ MHz.

condition $\hat{\mathbf{k}}_{ta} = -\hat{\mathbf{k}}_{ta}$ will no logger hold true and σ_{hh} will rapidly decrease. For σ_{vv} the same peak can be seen more clearly and has a value much higher than anything else in Figure 4.3b. When it comes to σ_{hv} and σ_{vh} they are 0 at $\theta_c = 30$ when $\phi_c = \pm 180°$. This does not mean that having $\hat{\mathbf{k}}_{ta} = -\hat{\mathbf{k}}_{ta}$ does not affect σ_{hv} and σ_{vh}. This is because the $\mathbf{S}_0$ matrix, presented in equation (3.3), has the components $S_{hv} = S_{vh} = 0$ for $\phi_c = 180°$ and $\phi_c = 0°$. Therefore, when ϕ_c is close to 180°, the same peak values that is seen in the upper corners of Figure 4.4 for σ_{hh} and σ_{vv}, can be seen for σ_{hv} and σ_{vh}.

Further, in Figure 4.4a, it can be seen that σ_{hh}, for $\phi_c = \pm 90°$ and starting at $\theta_c = 0°$, seems to decrease when θ_c increases initially but as θ_c increases further, σ_{hh} will start to increase. The reason for this, as can be seen in Figure 4.2, is that σ_{vv} is generally greater than σ_{hh} for frequencies around 150 MHz. Then, if $\phi_c = \pm 90°$ and θ_c is increased, the tree in the model will start to lie down and the horizontal electrical field component will start to align with the tree axis. When this is the

case, the horizontal component of the wave will be reflected as if a part of it is aligned with the tree and σ_{hh} will increase.

4.1.5 Backscattering with and without tree branches

The backscattering from a tree is not only dependent on the tree trunk but also on the branches. The backscattering from the branches varies with the angle of the branch axis relative the incident wave propagation direction. This is because the scattering of the cylinder used to approximate the branch varies with the incident direction of the wave as can be seen for the trunk in Figure 4.4. Figure 4.5 shows σ_{hh} and σ_{vv} calculated according to equation (2.13), for tree model 1 described in Section 3.2.3 with and without tree branches. If one calculates the volume of the tree trunk it becomes approximately 0.394 m^3 and the branch volume becomes 0.141 m^3.

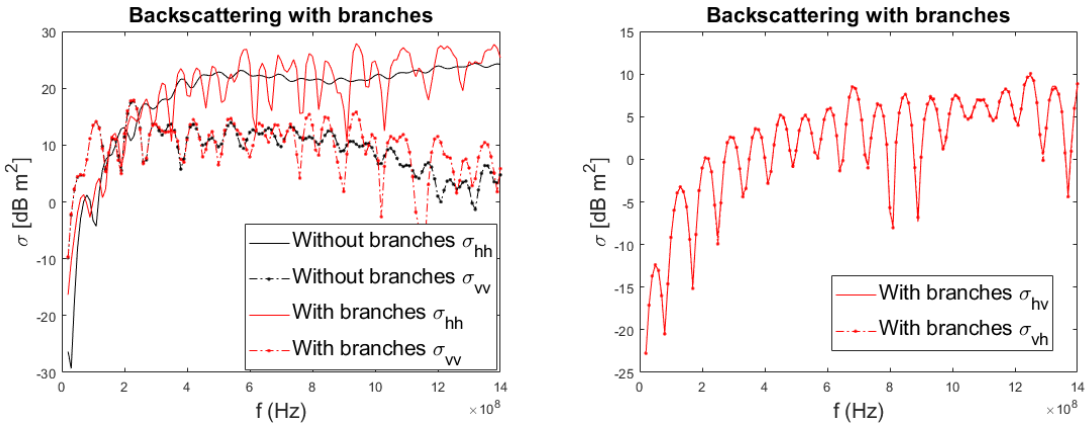

(a) (b)

Figure 4.5: The values of σ_{hh}, σ_{vv}, σ_{hv} and σ_{vh} were plotted against the frequency for tree model 1, described in Section 3.2.3. The radar cross sections were computed with and without tree branches and the branches were placed according to Section 3.2.3. The values were computed using $\theta_g = 0°$, $\phi_g = 0°$, $\theta_c = 0°$, $\phi_c = 0°$, $\theta_i = 60°$ and $\epsilon_r = 12.7 - j2.1$.

The tree branches' directions and heights were randomly decided as described in Section 3.2.3. After performing computations for multiple random placements and directions of the branches, it was obvious that the height of the branches and their direction affected the backscattering. In most cases the resulting σ_{hh} and σ_{vv} from trees with branches was similar to the σ_{hh} and σ_{vv} from trees without branches in Figure 4.5a. The value of σ for trees with branches in Figure 4.5a usually fluctuate around the value of σ for trees without branches. But in some rare cases, σ for trees with branches would be a lot greater and in other rare cases almost the same as the σ without branches. The reason behind those rare cases was when multiple branches had inclinations that allowed for unusually large or small backscattering.

In almost all placements of the branches it could be seen that σ_{vv} for a tree with and without branches had almost the same value for the lower frequencies. This is because the reflection from a polarization in the same direction as the tree

axis is far greater, for the lower frequency's, than the reflection from a polarization orthogonal to the tree axis. The tree trunk has an axis that is orthogonal to the horizontal polarization of the incident wave and therefore, for low frequencies, gives greater backscattering for the vertical polarization than the horizontal polarization. However, the branches' axes are not in the incidents wave's vertical polarization direction and will therefore give a smaller backscattering in comparison to the tree trunk for low frequencies.

Using the specific setup described in Figure 4.5, σ_{vh} and σ_{hv} will become zero for the tree without branches because neither the ground nor the trunk changes polarization of the wave. For the tree with branches σ_{vh} and σ_{hv} will not become zero because of the scattering of the branches. The computed σ_{vh} is almost the same as the computed σ_{hv}.

4.2 Backscattering from a forest

From the computed radar cross sections for a plane wave incident against a single trunk, it is seen that σ_{hh} is larger than σ_{vv} for high frequencies but smaller for low frequencies, see Subsection 4.1.2. The results have also shown that the slope of the ground have great effect on the RCS. In fact, as can be seen in Figure 4.3 and 4.4, for certain angles the amplitude can vary greatly for small changes in either the ground slope or the tree inclination. This will greatly effect the forest calculations since a single tree with the same size as the average tree, can give a reflection several times as large as other trees with the same size for certain slopes. Similarly, other slopes may cause a tree to barely scatter anything at all and therefore contribute several times less than the average trees of the same size.

There are many parameters that can be changed in the computation of the backscattering from a forest, allowing for simulation of a wide variety of real world cases. For more detailed explanations, see Section 3.3.2. However, for the forest the parameters that we will vary is the constant X, introduced in Section 3.1.1, that relates the cylinder length to the cylinders radius, the antenna position and ϵ_r. Because of positive and destructive interference between the backscattered waves, small changes in the antenna position may affect the backscattering more than expected.

4.2.1 Forest backscattering using different cylinder lengths

Figure 4.6 shows how σ_{tot}/R^4, presented in equation (3.11), varies for different X,introduced in Section 3.1.1, as the frequency changes. The figure shows $X = 20$, $X = 40$ and $X = 10$, where X relates the cylinder length to the cylinders radius. When using $X = 20$ the forest approximation is made up of approximately 6000 cylinders, when $X = 40$ approximately 11000 cylinders and when $X = 10$ approximately 3000 cylinders. Since the forest is made up of 748 trees, this corresponds to approximately 8, 15 and 4 cylinders per approximated tree.

The variation of the backscattering depending on the cylinder size for one tree trunk has been tested and studied in Section 4.1.2 and Figure 4.2. There, it was found that when computing an approximate value for σ_{hh} there was no need to use

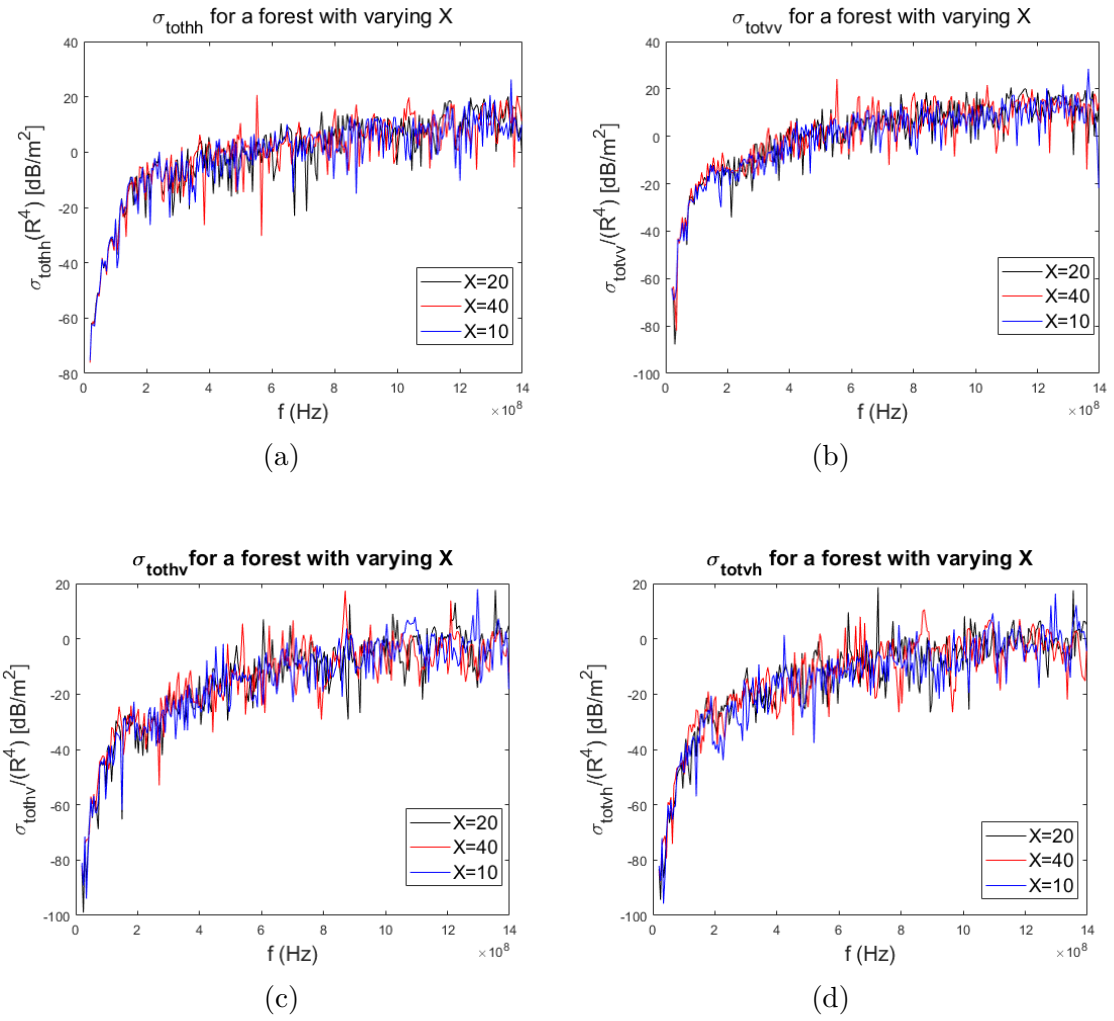

Figure 4.6: The values of σ_{tothh}/R^4, σ_{totvv}/R^4, σ_{tothv}/R^4 and σ_{totvh}/R^4 are shown in subplot (a) – (d), respectively against the frequency for different values of X. X relates the cylinder length to the cylinders radius. When using $X = 20$ the forest approximation is made up of approximately 6000 cylinders, when $X = 40$ approximately 11000 cylinders and when $X = 10$ approximately 3000 cylinders. The figures was created using $\epsilon_r = 12.7 + j2.1$ and the antenna position $(79.5, -8, 50)$.

more than 5 to 10 cylinders per tree. However, when more cylinders where used more fluctuations can be seen allowing more exact calculations for specific frequencies. Prominent was also that independent of the number of cylinder used, σ_{hh} follows the same general curve with the only difference of more or less fluctuations.

In Figure 4.6a it can be seen that the value of σ_{tothh}/R^4 shows several similarities to the value of σ_{hh} in Figure 4.2. One similarity is the independence of the number of cylinders used σ_{tothh}/R^4 follows more or less the same curve for all values of X, with the only difference of how it fluctuates. Another similarity is the shape of the curve which shows that when the f goes from 100 MHz to 400 MHz, both σ_{hh}, from Figure 4.2, and σ_{tothh}/R^4, from Figure 4.6a, increases with approximately 25 dB. This shows a clear connection between the reflection of a single tree and the reflections from multiple trees combined.

However, something different is that σ_{tothh}/R^4 fluctuates equally much both when a tree is approximated with 15 and 4 cylinders. This is because the fluctuations are dependent on the total number of cylinders rather than the number of cylinder for a single tree. The reason that the forest models σ_{tothh}/R^4 value fluctuate more than the single tree models σ_{hh} value is because the forest have more cylinders than the model of a single trunk.

Another difference between Figure 4.6 and Figure 4.2 is that the size of σ_{tothh}/R^4 is approximately the same as the size of σ_{totvv}/R^4. In the case of a single tree it is for the higher frequencies obvious that $\sigma_{hh} > \sigma_{vv}$. This signifies that for small inclinations of the ground and trees, the vertical polarization will decrease less than the horizontal polarization. Indications of this can also be seen in Figure 4.3 where σ_{hh} has its maximum value then there are no inclination while σ_{vv} does not have a maximum value for no inclination. The fluctuation in the σ_{totvv}/R^4 value is due to the same reason as the fluctuation in σ_{tothh}/R^4.

The value of σ_{tothv}/R^4 and σ_{totvh}/R^4 can be seen to be very similar in Figure 4.6. The reason these are not zero, as σ_{vh} and σ_{hv} were in Section 4.1.2, is because the ground and trees have different inclinations in the forest. How the ground and tree inclination affects σ_{tothv}/R^4 and σ_{totvh}/R^4 can be estimated from Figure 4.3 and 4.4. Worth noting is that both σ_{tothv}/R^4 and σ_{totvh}/R^4 is much smaller than σ_{tothh}/R^4 and σ_{totvv}/R^4.

4.2.2 Forest backscattering for different antenna positions

Figure 4.7 shows how σ_{tot}/R^4, presented in equation (3.11), depends on the frequency for different antenna positions. The exact position for the antenna in the forest is not known but has been estimated to be at $(79.5, -8, 50)$ meters (see Figure 3.3). The results for this position can be seen in Figure 4.7 as 'specific position´. The figure also shows the average result of eight antenna positions around the estimated antenna position. The eight used position are all possible combinations of $(79.5 \pm 0.5, -8 \pm 0.5, 50 \pm 0.5)$. The figure is created using $X = 20$, which means that the forest model is approximately built up using 6000 cylinders.

Figure 4.7 indicates that the average value of σ_{tot}/R^4 for the eight antenna positions has less fluctuations than the value for an individual antenna, as expected. This is because the fluctuation is reduced in the average process since the individual values have fluctuation at different frequencies. However, both curves can be seen to vary similarly with the exception of the fluctuations. This continues to be true even for other antenna positions close to the estimated antenna position. This indicates that the general curve shape of the backscattering is not dependent on the exact antenna position. This is advantageous, because it means that if one in a real scenario slightly moves the antenna, it should not affect the result of the measurements to become totally different. It also indicates, that even if we in our computations do not know the exact antenna position, the estimated position should give a result similar to the result given by the exact antenna position.

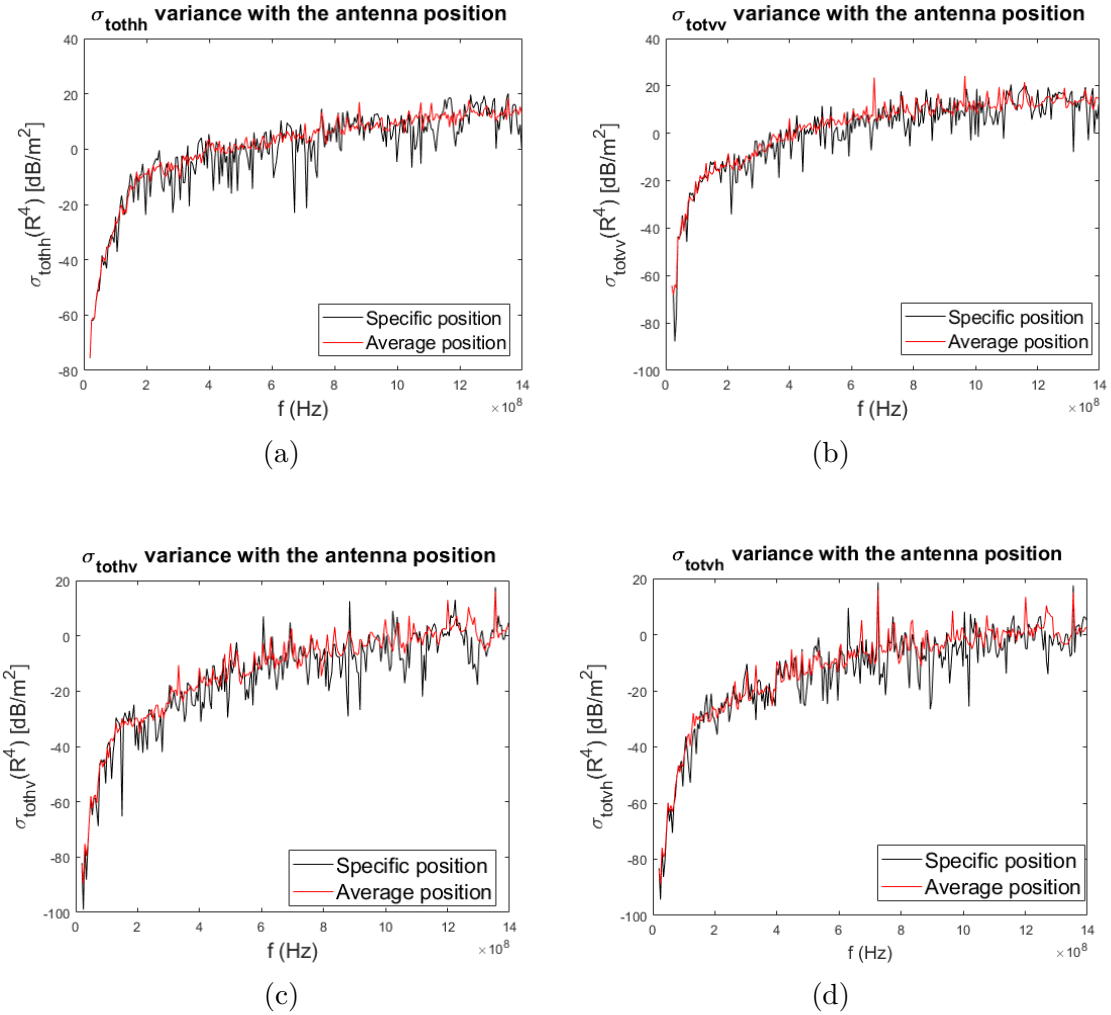

Figure 4.7: The figure shows σ_{tot}/R^4 for different polarizations against the frequency and for different antenna positions. The exact antenna position in the forest is not known but has been estimated to be at position $(79.5, -8, 50)$ (black line). The result at this antenna position is in the figures compared to the average results of eight different antenna positions $(79.5 \pm 0.5, -8 \pm 0.5, 50 \pm 0.5)$ (red line). The figure was created using $X = 20$ which means that the forest is approximately made up of 6000 cylinders, and using $\epsilon_r = 12.7 + j2.1$.

4.2.3 Forest backscattering with attenuation

Figure 4.8 shows σ_{tot}/R^4, presented in equation (3.11), when the attenuation is included in the model. The figure shows two plots, one where the attenuation have been considered and one where the attenuation has not been considered. As can be seen in the figure, the value of σ_{tot}/R^4 has become noticeably lower for some frequencies when the attenuation has been included in the model. But for other frequencies the attenuation's influence cannot be seen as clearly and the reason for this is that the attenuation is frequency dependent as can be see in Appendix A.1 Figure A.1. In Figure A.1, it can be seen that the attenuation for the horizontal polarization is largest between 125 and 350 MHz. Indications of this can also be

seen in σ_{tothh}/R^4, in Figure 4.8a, where the red curve is significantly lower than the black one for the frequencies 125-350 MHz. This shows that adding attenuation to the computation has a noticeable effect in diminishing the RCS. However, this is not always the case, at some frequencies σ_{tothh}/R^4 with attenuation is larger than it is without attenuation. This has to do with destructive and constructive interference of waves that scatters towards the antenna with different polarizations. For some frequencies, adding attenuation could diminish the destructive interference and therefore cause σ_{tothh}/R^4 to increase.

Similar observations can be made for σ_{totvv}/R^4 in Figure 4.8b, which decreases more for some frequencies than for other frequencies due to the attenuation being frequency dependent, as can be see in Appendix A.1, Figure A.1.

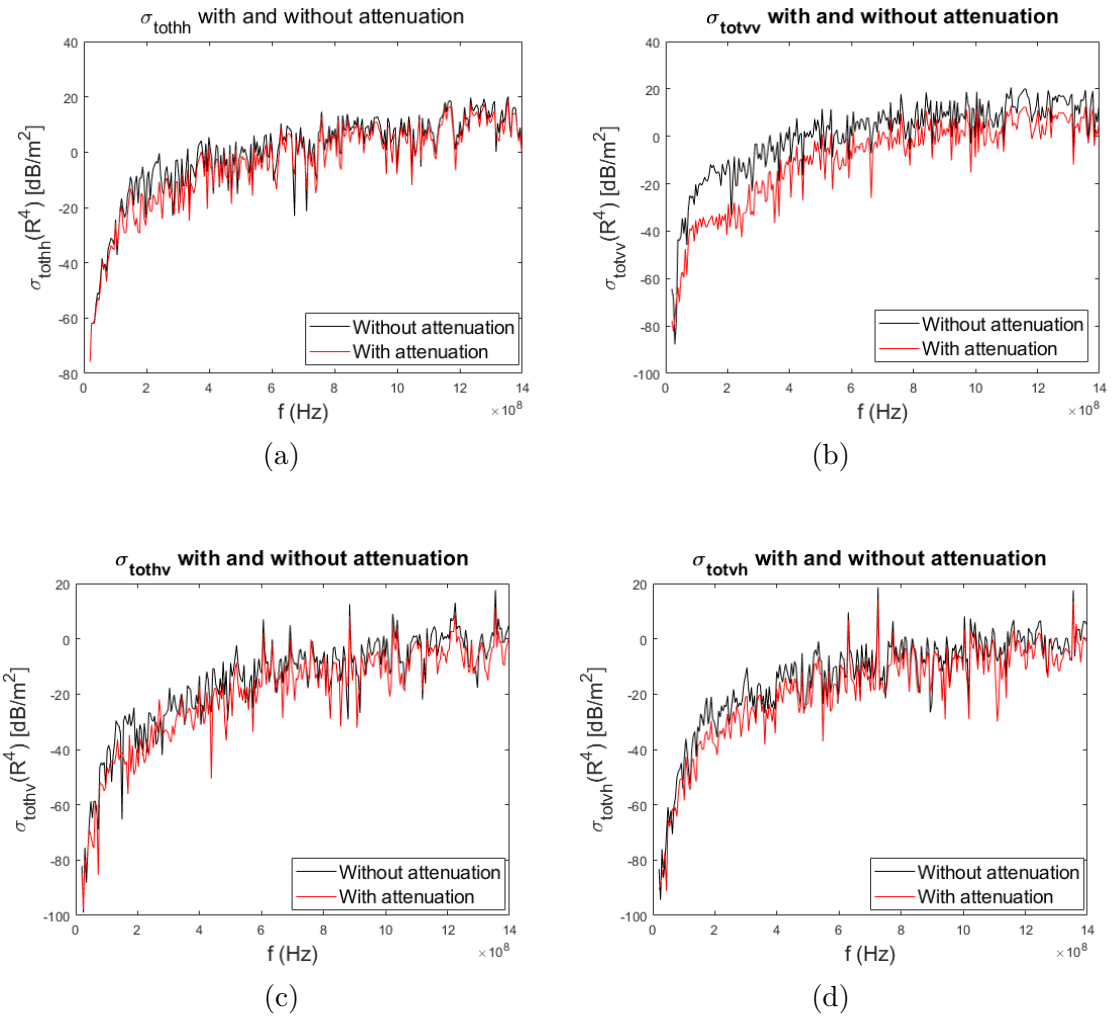

Figure 4.8: The values of σ_{tothh}/R^4, σ_{totvv}/R^4, σ_{tothv}/R^4 and σ_{totvh}/R^4 with and without attenuation are shown in subplot (a) – (d), respectively against the frequency. The figures was created using $X = 20$, $\epsilon_r = 12.7 + j2.1$ and the antenna position $(79.5, -8, 50)$.

4.2.4 Forest backscattering for different moisture contents

Knowing how the backscattering varies depending on the ground and tree's moisture content is advantageous when performing backscattering measurements. This is because the moisture content in the trees and earth changes with the weather and season. As the moisture content in wood and soil changes, the permittivity will also change according to what is presented in Appendix A.2 (see Figure A.2) and A.3 (see Figure A.3). Figure 4.9 shows how the computed σ_{tot}/R^4 varies for the forest as the tree and ground moisture content changes. The figure is created without considering any attenuation, using $f = 435$ MHz, $X = 40$ that relates a cylinders length to it's radius, which means that the forest model is approximately build up using 3000 cylinders.

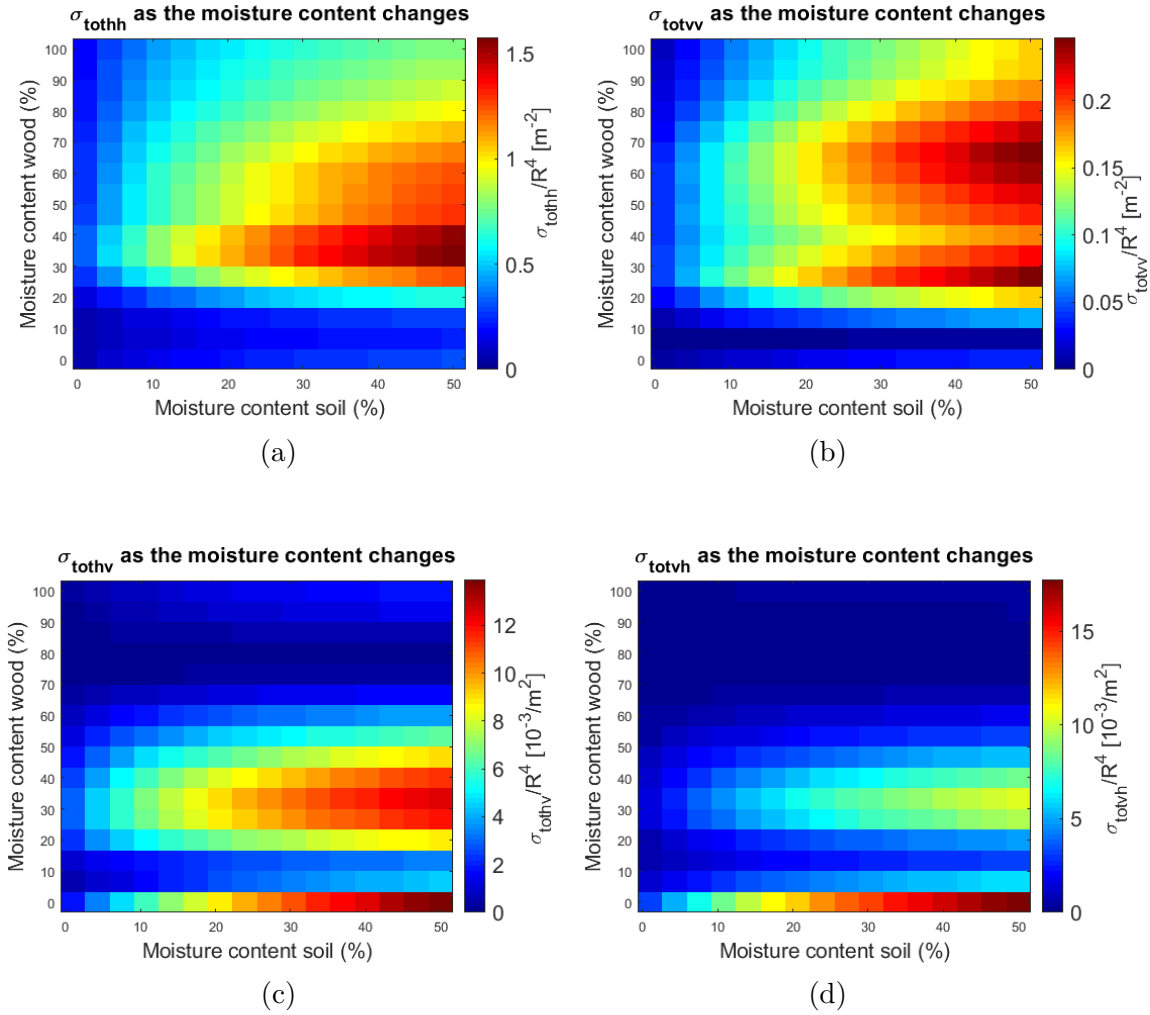

Figure 4.9: The values of σ_{tothh}/R^4, σ_{totvv}/R^4, σ_{tothv}/R^4 and σ_{totvh}/R^4 are shown in subplot (a) – (d), respectively against the moisture content percentage in the soil and the wood. The figures were created using $X = 40$, $f = 435$ MHz, the antenna position $(79.5, -8, 50)$ and permittivities corresponding to the moisture content percentage, see Appendix A.2 and A.3.

The values of σ_{tot}/R^4, in Figure 4.9, can for all polarization's and all wood

moisture content be seen to be increasing as the soil's moisture contents increases. This is because of the fact that as the soil's moisture content increases, the grounds permittivity will increase, see Appendix A.3 (see Figure A.3). This causes $|\Gamma_{hh}|$ and $|\Gamma_{vv}|$, see equation (2.7) and (2.8), to increase for almost all incidence angles which results in that σ_{tot}/R^4 increases, see equation (3.11) and (3.3).

5
Conclusion

The goal of this thesis was to create an electromagnetic model of a forest, calculate the backscattering from this forest and determine whenever the GRG approximation or truncated infinite cylinder approximation can be used. It is concluded that the truncated infinite cylinder approximation is a better approximation in the model due to the constraints of the GRG approximation. The latter constraints constraints are that $ka << 1/\sqrt{\epsilon_r}$ and $h > 20a\sqrt{\epsilon_r}$, and a consequence of this is that the GRG can not be used for all frequencies of interest (20-1400 MHz). Another consequence is that the cylinder length, that needs to be used when approximating the forest, would become too long which will make it difficult, if even possible, to create a good forest approximation. As a consequence of this, only the truncated infinite cylinder approximation was used in the model of this thesis.

In the creation of the forest model, the cylinder data presented in Section 3.1 were used even if this data contained a few irregularities. An example of an irregularity was that cylinders with different radii and inclinations could overlap one another. This means that one of the cylinders will contain data that does not correspond to the real tree at the overlapping point. In addition, several approximations were made to get rid of the overlap of cylinders and fill in the empty space between the cylinders. Since the original cylinder data already contained approximations, and then more approximations where made, it is likely that the final forest model is a bit different from the real forest. But when looking at Section 4.2.1 and 4.2.2, it can be seen that moving the antenna position slightly or changing the cylinder approximation only affects the backscatter's fluctuation, but not it's mean value. This indicates that the model is quite stable, and most likely, the general curve's shape of the backscattering would not change much even if a more perfect geometrical forest model could have been made.

The effect of changing the size of a tree, studied in Section 4.1.1, gave the expected result that large trees gives more backscattering than small trees. However, a bit unexpected was that for some frequencies, σ_{vv} was larger for a small tree than for a large tree. A direct relationship between tree size and tree volume or tree size and tree surface area could however not bee seen.

It was in Section 4.1.3 and 4.1.4 found that changing the tree inclination or ground slope slightly can significantly change the backscattering. It can therefore be concluded that tree inclination and ground slope are extremely important factors when measuring or computing backscattering.

Bibliography

[1] G. Sandberg (2013), “Estimation of forest biomass and Faraday rotation using ultra high frequency synthetic aperture radar ”, PhD thesis Chalmers University of Technology, Department of Space, Earth and Environment, Gothenburg, Sweden, ISBN: 978-91-7385-912-7

[2] B. Hallberg (2007), “Synthetic-aperture radar imaging of forests in the VHF and UHF bands: Electromagnetic models and data analysis”, PhD thesis-Chalmers University of Technology, Department of Space, Earth and Environment, Gothenburg, Sweden, ISBN: 978-91-7291-941-9

[3] M. A. Richards, J. A. Sheer, W. A. Holm, (2010) "Principles of modern radar, basic principles", ISBN 978-1-891121-52-4, chapter 1 and 2 , second edition, pp. 1-85

[4] K. Olofsson and J. Holmgren (2016) "Single Tree Stem Profile Detection Using Terrestrial Laser Scanner Data, Flatness Saliency Features and Curvature Properties", Forests, 7 (9), 207

[5] V. Edgren and P. Nylinder (1949), “Funktioner och tabeller för bestämning av avsmalning och formkvot under bark tall och gran i norra och södra Sverige ”, Swedish Forest Res. Inst., Stockholm, Sweden, Rep. 36:3

[6] G. I. Torgovnikov (1993)," Dielectric Properties of Wood and Wood-Based Materials", State University of New York, College of Environmental, Science and Foresty, Syracuse, NY 13210, USA, ISBN-13 :978-3-642-77455-3

[7] G. Smith-Jonforsen, L. M. H. Ulander and Xianyun Luo, (2005), “Low VHF-Band Backscatter From Coniferous Forests on Sloping Terrain”, IEEE TRANSACTIONS ON GEOSCIENCE AND REMOTE SENSING, VOL. 43, NO. 10

[8] T. B.A Senior, K. Sarabandi (1990), "Scattering models for point targets" in *Radar Polarimetry for Geoscience Application*, second edition, editors Fawwaz T. Ulaby, Charles Elachi, ISBN:0-89006-406-7

[9] R. Schiffer, and K. O. Thielheim (1979), "Light scattering by dielectric needles and disks" Journal of Applied Physics 50, pp 2476-2483

[10] M. A. Karam A. K. Fung (1988), “Electromagnetic scattering from a layer of finite length, randomly oriented, dielectric, circular cylinders over a rough interface with application to vegetation”, International Journal of Remote Sensing, 9:6, pp 1109-1134,

[11] M. A. Karam, A. K. Fung, and Y. M. M. Antar, (1988) “Electromagnetic wave scattering from some vegetation samples,” IEEE Trans. Geosci. Remote Sens, vol. 26, no. 6, pp. 799–808

[12] J. M. Stiles and K. Sarabandi, (1996), “A scattering model for thin dielectric cylinders of arbitrary cross section and electrical length,” IEEE Trans. Antennas Propagat., vol. 44, no. 2, pp. 260–266

[13] Y. C. Lin and K. Sarabandi (1995), “Electromagnetic scattering model for a tree trunk above a tilted ground plane,” IEEE Trans. Geosci. Remote Sens. vol. 33, no. 4, pp. 1063–1070

[14] M. A. Karam and A. K. Fung (1983), “Scattering from randomly oriented circular discs with application to vegetation”, Radio Science, Volume 18, Number 4, pages 557-565

[15] J. C. Maxwell (1865), "A dynamical theory of the electromagnetic field" in *philosophical transactions of the royal society of London*, vol. 155, pp. 459-512

[16] S. J. Orfanidis (2002), "Maxwell's Equations" in *Electromagnetic Waves and Antennas*, pp. 2-35

[17] D. K. Cheng (2014), "Time-Varying Fields and Maxwell's Equations" in *Time-Varying Fields and Maxwell's equations*, second edition, pp. 307-353

[18] D. K. Cheng (2014), "Plane Electromagnetic Waves" in *Time-Varying Fields and Maxwell's equations*, second edition, pp. 354-426

[19] IEEE standard letter designations for radar-frequency bands, IEEE-SA Standards Board, ISBN 0-7381-3356-6

[20] E. F. Knott, J. F. Shaeffer, Michael T. Tuley (2004), "Physics and Overview of Electromagnetic Scattering" in *Radar Cross Section*, second edition, ISBN:9781891121258

[21] E. F. Knott (1990), "Radar Cross Section" in *Radar Handbook*, second edition, ISBN 0-07-057913-X

[22] H, Hellsten (2017), "Meter-Wave Synthetic Aperture Radar for Concealed Object Detection ", ISBN-13 :978-1-63081-025-2, pages 110-119

[23] Torgovnikov, Grigory (1993), "Dielectric Properties of Wood and Wood-Based Materials",Central Scientific Research Institute of Forest Industry, ISBN-13 :978-3-642-77455-3

[24] F. Ulaby (2014), "Microwave Dielectric Properties of Natural Earth Materials" in Microwave Radar and Radiometric Remote Sensing, ISBN 978-0-472-11935-6

A

Appendix

A.1 Attenuation due to trees and branches

When an electromagnetic wave passes though a forest, it will be partly scattered by trees and branches. But parts of the electromagnetic wave will continue propagating without changing direction. However, this part will attenuate more and more the longer the wave propagates though the forest. The mathematical method to calculate the attenuation is presented below, for the more interested reader a theoretical description of the physics behind the attenuation process can be found in [22]. The mathematical equations used when calculating the attenuation A, when a wave travels to the ground and back, is as follows [22]

$$\mathbf{I} = \begin{bmatrix} 1 & 0 \\ 0 & 1 \end{bmatrix} \tag{A.1a}$$

$$K = \frac{2\pi}{\lambda} \tag{A.1b}$$

$$K_{ABR} = K * R_{ADBR} \tag{A.1c}$$

$$K_{AST} = K * R_{ADST} \tag{A.1d}$$

$$R_I = \sqrt{\epsilon_r \mu_r} \tag{A.1e}$$

$$B_{DENS} = \frac{B_{PERT}}{2HS_{EP}} \tag{A.1f}$$

where B_{PERT} is the number of branches per tree, H is the tree height, S_{EP} is the distance between the trees, R_{ADBR} is the average branch radius and R_{ADST} is the radius of the tree. Furthermore, θ is the incidence angle and χ is the angle between the branches and the tree. Then

$$A_H = \sum_{i=1}^{N} 2A_A(i) \tag{A.2a}$$

$$B_H = \sum_{i=1}^{N} 2B_B(i) \tag{A.2b}$$

where

$$N = \text{round}(A_K) \tag{A.3a}$$
$$J(i) = J_{(i-1)}(A_K) \tag{A.3b}$$
$$J_M(i) = J_{(i-1)}(R_I A_K) \tag{A.3c}$$
$$H(i) = H^{(1)}_{(i-1)}(K_{ARB}) \tag{A.3d}$$
$$H_M(i) = H^{(1)}_{(i-1)}(R_I K_{ARB}) \tag{A.3e}$$
$$D_J(i) = J_1(A_K) \quad \text{for } i = 1 \tag{A.3f}$$
$$D_J(i) = (J_{(i-2)}(A_K) - J_i(A_K))/2 \quad \text{for } i \neq 1 \tag{A.3g}$$
$$D_{JM}(i) = J_1(R_I A_K) \quad \text{for } i = 1 \tag{A.3h}$$
$$D_{JM}(i) = (J_{(i-2)}(R_I A_K) - J_i(R_I A_K))/2 \quad \text{for } i \neq 1 \tag{A.3i}$$
$$D_H(i) = H^{(1)}_1(R_I A_K) \quad \text{for } i = 1 \tag{A.3j}$$
$$D_{HM}(i) = (H^{(1)}_{(i-2)}(R_I A_K) - H^{(1)}_i(R_I A_K))/2 \quad \text{for } i \neq 1 \tag{A.3k}$$
$$B_B(i) = \frac{J_M(i)D_J(i) - R_I D_{JM}(i)J(i)}{R_I H(i)D_{JM}(i) - D_H(i)J_M(i)} \tag{A.3l}$$
$$A_A(i) = \frac{D_{JM}(i)J(i) - R_I J_M(i)D_J(i)}{R_I D_H(i)J_M(i) - H(i)D_{JM}(i)} \tag{A.3m}$$

where $J_n()$ is n-order order Bessel function of first kind, $H^{(1)}_n()$ is a n-order order Bessel function of third kind and A_K can represent either K_{ABR} or K_{AST}. Furthermore,

$$E_{BR} = (0, -\sin(\chi), \cos(\chi)) \quad \text{for } A_K = K_{ABR} \tag{A.4a}$$
$$E_{BR} = (0, 0, 1) \quad \text{for } A_K = K_{AST} \tag{A.4b}$$
$$A_{TE} = j * \sqrt{2} A_H / K \tag{A.4c}$$
$$A_{TM} = \sqrt{2} B_H / K \tag{A.4d}$$
$$P_{HI}(L) = \pi L / 180 \tag{A.4e}$$
$$E_P(L) = [sin(\theta)sin(P_{HI}(L)), -sin(\theta)cos(P_{HI}(L)), cos(\theta)] \tag{A.4f}$$
$$V_{ERT} = [0, 0, 1] \tag{A.4g}$$
$$P_{XC1}(L) = E_P(L) \times E_{BR}; \tag{A.4h}$$
$$A_{BSPXC}(L) = \sqrt{P_{XC1}(L) \cdot P_{XC1}(L)} \tag{A.4i}$$
$$P_{XC}(L) = P_{XC1}(L) / A_{BSPXC}(L); \tag{A.4j}$$
$$V_{DOTPXC}(L) = V_{ERT} \cdot P_{XC}(L) \tag{A.4k}$$
$$C_{OSPSI}(L) = |V_{DOTPXC}(L)| \tag{A.4l}$$
$$S_{INPSI}(L) = \sqrt{1 - (C_{OSPSI}(L))^2} \tag{A.4m}$$
$$A_{BR11}(L) = A_{TM}(C_{OSPSI}(L))^2 + A_{TE}(S_{INPSI}(L))^2 \tag{A.4n}$$
$$A_{BR12}(L) = (A_{TM} - A_{TE})C_{OSPSI}(L)S_{INPSI}(L) \tag{A.4o}$$
$$A_{BR21}(L) = A_{BR12} \tag{A.4p}$$
$$A_{BR22}(L) = A_{TE}(C_{OSPSI}(L))^2 + A_{TM}(S_{INPSI}(L))^2. \tag{A.4q}$$

Using $A_K = K_{ABR}$ in equation (A.4), the next step in the calculations will be

$$A_{VABR1} = \begin{bmatrix} \sum_{L=1}^{60} A_{BR11}(L) & \sum_{L=1}^{60} A_{BR12}(L) \\ \sum_{L=1}^{60} A_{BR21}(L) & \sum_{L=1}^{60} A_{BR22}(L) \end{bmatrix} /60 \tag{A.5a}$$

$$A_{VABR2} = \begin{bmatrix} \sum_{L=61}^{90} A_{BR11}(L) & \sum_{L=61}^{90} A_{BR12}(L) \\ \sum_{L=61}^{90} A_{BR21}(L) & \sum_{L=61}^{90} A_{BR22}(L) \end{bmatrix} /30 \tag{A.5b}$$

$$A_{VABR4} = \begin{bmatrix} \sum_{L=91}^{120} A_{BR11}(L) & \sum_{L=91}^{120} A_{BR12}(L) \\ \sum_{L=91}^{120} A_{BR21}(L) & \sum_{L=91}^{120} A_{BR22}(L) \end{bmatrix} /30 \tag{A.5c}$$

$$A_{VABR5} = \begin{bmatrix} \sum_{L=121}^{180} A_{BR11}(L) & \sum_{L=121}^{180} A_{BR12}(L) \\ \sum_{L=121}^{180} A_{BR21}(L) & \sum_{L=121}^{180} A_{BR22}(L) \end{bmatrix} /60 \tag{A.5d}$$

$$\tag{A.5e}$$

and using $A_K = K_{AST}$ in equation (A.4), the next step in the calculation will be

$$A_{VABR3} = \begin{bmatrix} A_{BR11}(0) & A_{BR12}(0) \\ A_{BR21}(0) & A_{BR22}(0) \end{bmatrix} \tag{A.6}$$

The scattering and attenuation can then be calculated as

$$S_{CATT1} = (\mathbf{I} + S_{EP} B_{DENS} A_{VABR2}/4)(\mathbf{I} + S_{EP} B_{DENS} A_{VABR1}/4) \tag{A.7a}$$

$$S_{CATT2} = (\mathbf{I} + S_{EP} B_{DENS} A_{VABR4}/4)((\mathbf{I} + A_{VABR3}/S_{EP})(S_{CATT1})) \tag{A.7b}$$

$$S_{CATT3} = (\mathbf{I} + S_{EP} B_{DENS} A_{VABR5}/4) S_{CATT2} \tag{A.7c}$$

$$S_{CATT0} = |S_{CATT3}|.^2 \tag{A.7d}$$

$$D_{EPTH} = \frac{H}{\cos(\theta)} \tag{A.7e}$$

$$S_{CATT} = S_{CATT0}.^{2D_{EPTH}/S_{EP}} A = |S_{CATT}|^d \tag{A.7f}$$

In Figure A.1 the attenuation due to the trees is plotted against the frequency for a wave traveling though a forest.

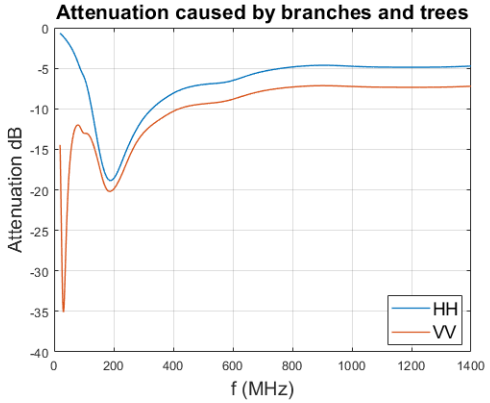

Figure A.1: The wave's total attenuation due to the trees when traveling though a forest to the ground and back, while $B_{PERT} = 50$, $H = 18.7$ m, $\theta = 60°$, $\chi = 90°$, $S_{EP} = 4.3$ m, $R_{ADBR} = 0.015$ m and $R_{ADST} = 0.0903$ m.

A.2 The permittivity's dependence on the wood moisture content

A tree trunk's dielectric properties are dependent on how much water is in the trunk. A measure of the amount of water in the trunk is the wood moisture content, which is calculated as the mass of the water in the trunks divided by what the trunks mass would have been without any water. The permittivity's dependence on the wood moisture is well explained in [23], and using this the permittivity (ϵ_r) of the wood is calculated as

$$\epsilon_r = \epsilon_{temp}(1 - jL) \tag{A.8}$$

where ϵ_{temp} and L for a horizontal polarization is defined as

$$\epsilon_{temp} = 0.001016 * m_c^2 + 0.03705 * m_c + 2.002 \tag{A.9a}$$

$$L = 0.115 * e^{0.003321 m_c} - 0.09049 * e^{-0.07819 * m_c}. \tag{A.9b}$$

This relation is approximately valid for Norway spruce when the temperature is 20° C and the frequency is 100 MHz, but the value of the permittivity should only change slightly as frequency is increased to 1 GHz. The variable m_c represents the wood moisture content in percentage. In Figure A.2, m_c is plotted against ϵ_r for horizontal polarization. For vertical polarization, ϵ_r will become different but in

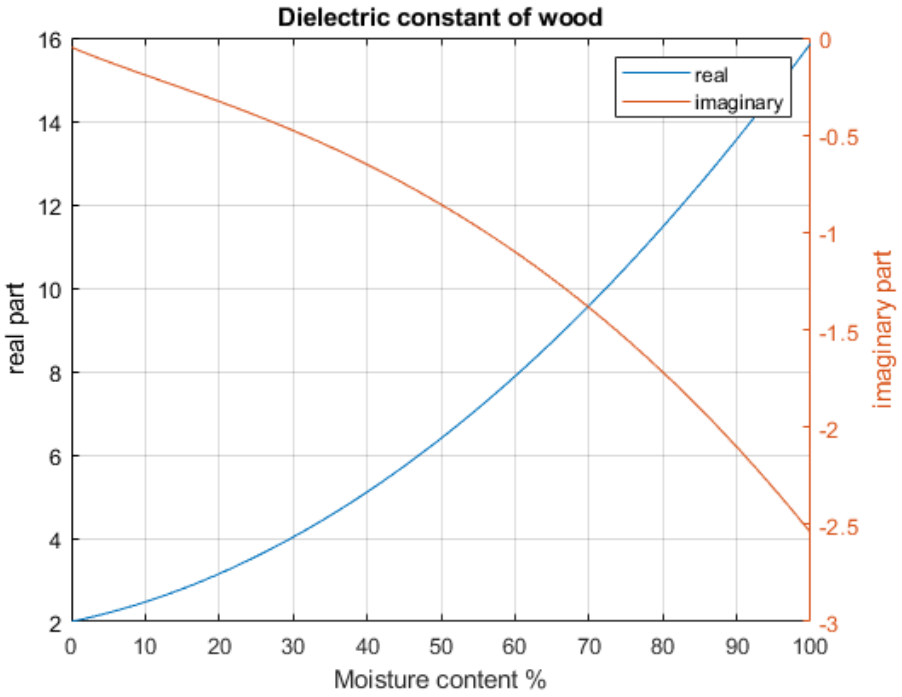

Figure A.2: The permittivity of Norway spruces against moisture content, when the temperature is 20° C and the frequency is 100 MHz

this thesis, ϵ_r will only be calculated for the horizontal polarization. This is because the cylinder scattering model used (see Subsection 2.5.2) does not work when ϵ_r is different for different polarization directions.

A.3 The permittivity's dependence on the soil moisture content

The dielectic properties of the ground is dependent on how much water is in the soil. A measure for the amount of water in the ground is the soil moisture content which is calculated as the mass of the water in the soil divided by what the soil mass would have been without any water. The permittivity's dependence on soil moisture content for the ground is well explained in [24], and using this the permittivity (ϵ_r) of the soil is calculated as

$$\epsilon_r = \epsilon_{soilreal} + j\epsilon_{soilimag} \tag{A.10}$$

where $\epsilon_{soilreal}$ and $\epsilon_{soilimag}$ is defined as

$$\epsilon_{soilimag} = (m_v^{\beta_2})\epsilon_{Wimag} \tag{A.11a}$$

$$\epsilon_{soilreal} = 1.15(1 + 0.66p_b + m_v^{\beta_1}(\epsilon_{Wreal}^{\alpha} - m_v)^{1/\alpha} - 0.68 \tag{A.11b}$$

$$\epsilon_{Wimag} = (2\pi f\tau_W)(\epsilon_{w0} - \epsilon_{Winf})/(1 + (2\pi f\tau_W)^2) + ((2.65 - p_b)/(2.65m_v))(\sigma/(2\pi\epsilon_0 f)) \tag{A.11c}$$

$$\epsilon_{Wreal} = \epsilon_{Winf} + (\epsilon_{w0} - \epsilon_{Winf})/(1 + (2\pi f\tau_W)^2) \tag{A.11d}$$

$$\sigma = 0.0467 + 0.22p_b - 0.411S + 0.661C \tag{A.11e}$$

$$\alpha = 0.65 \tag{A.11f}$$

$$\beta_1 = 1.27 - 0.519S - 0.152C \tag{A.11g}$$

$$\beta_2 = 2.06 - 0.928S - 0.255C \tag{A.11h}$$

$$p_b = 1.7 \tag{A.11i}$$

$$\tau_W = (1.1109 * 10^6 - 38240T + 693.8T^2 - 5.096T^3)/(2 * 10^{16}\pi) \tag{A.11j}$$

$$\epsilon_{Winf} = 4.9 \tag{A.11k}$$

$$\epsilon_{w0} = 88.045 - 0.4147 * T + (6.295 * 10^{-4}) * T^2 + (1.075 * 10^{-5}) * T^3 \tag{A.11l}$$

$$m_v = m_c/100 \tag{A.11m}$$

In the equations, T is the temperature in Celsius, f is the frequency, m_c represent the soil moisture content percentage, S is the mass fraction of sand and C is the mass fraction of clay.

Figure A.3 shows m_c against ϵ_r for $T = 20°$ C, $S = 0.5$, $C = 0.15$ and $f = 435$ MHz.

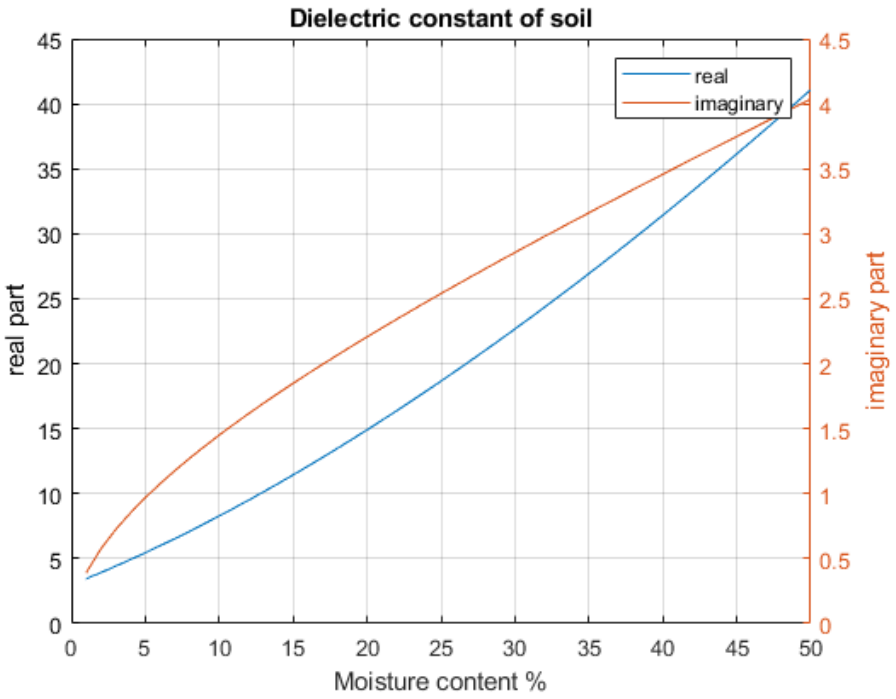

Figure A.3: The permittivity of soil plotted against moisture content, when $T = 20°C$, the mass fraction of sand $S = 0.5$, the mass fraction of clay $C = 0.15$ and $f = 435$ MHz